

APPENDIX E

MASTER

THESIS

PARAMETERIZATION OF NET RADIATION AT THE SURFACE
USING DATA FROM THE WANGARA EXPERIMENT

Submitted by

Roger T. Edson

Department of Atmospheric Science

In partial fulfillment of the requirements

for the Degree of Master of Science

Colorado State University

Fort Collins, Colorado

Summer, 1980

DISCLAIMER

This book was prepared as an account of work sponsored by an agency of the United States Government. Neither the United States Government nor any agency thereof, nor any of their employees, makes any warranty, express or implied, or assumes any legal liability or responsibility for the accuracy, completeness, or usefulness of any information, apparatus, product, or process disclosed, or represents that its use would not infringe privately owned rights. Reference herein to any specific commercial product, process, or service by trade name, trademark, manufacturer, or otherwise, does not necessarily constitute or imply its endorsement, recommendation, or favoring by the United States Government or any agency thereof. The views and opinions of authors expressed herein do not necessarily state or reflect those of the United States Government or any agency thereof.

DISTRIBUTION OF THIS DOCUMENT IS UNLIMITED

DISCLAIMER

This report was prepared as an account of work sponsored by an agency of the United States Government. Neither the United States Government nor any agency Thereof, nor any of their employees, makes any warranty, express or implied, or assumes any legal liability or responsibility for the accuracy, completeness, or usefulness of any information, apparatus, product, or process disclosed, or represents that its use would not infringe privately owned rights. Reference herein to any specific commercial product, process, or service by trade name, trademark, manufacturer, or otherwise does not necessarily constitute or imply its endorsement, recommendation, or favoring by the United States Government or any agency thereof. The views and opinions of authors expressed herein do not necessarily state or reflect those of the United States Government or any agency thereof.

DISCLAIMER

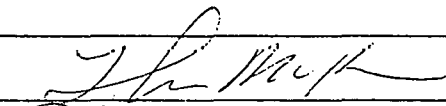
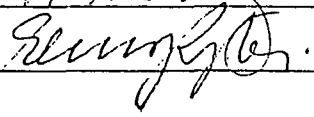
Portions of this document may be illegible in electronic image products. Images are produced from the best available original document.

COLORADO STATE UNIVERSITY

Summer 1980

WE HEREBY RECOMMEND THAT THE THESIS PREPARED UNDER OUR SUPERVISION
BY Roger T. Edson
ENTITLED PARAMETERIZATION OF NET RADIATION AT THE SURFACE USING DATA
FROM THE WANGARA EXPERIMENT
BE ACCEPTED AS FULFILLING IN PART REQUIREMENTS FOR THE DEGREE OF
MASTER OF SCIENCE

Committee on Graduate Work

<u></u>	<u>_____</u>
<u>Robert A. McNamee</u>	<u>_____</u>
<u></u>	<u>_____</u>
Adviser	

ABSTRACT OF THESIS

PARAMETERIZATION OF NET RADIATION AT THE SURFACE USING DATA FROM THE WANGARA EXPERIMENT

Hourly Wangara boundary layer data (Clark et al., 1971) is used to substantiate previously derived empirical equations of the surface radiation budget. These equations only require measurements taken by a surface observer in order to be evaluated. A parameterization was made for infrared (IR) radiation. From this procedure, a residual radiation was obtained from the measured daytime net radiation data in order to approximate short wave (SW) radiation. Diurnal trends in radiation and other related meteorological parameters were also evaluated.

For IR radiation, the Brunt equation was found to adequately represent effective radiation without clouds. IR attenuation (K-values) of 0.89, 0.64, and 0.51 were calculated for low, middle, and high clouds, respectively. While the value for high clouds was high, the values for middle and low clouds were found to be similar to previous studies. A mean K-value of 0.80 for all cloud conditions was also determined. For any type of cloudiness situation, an increase in cloud coverage attenuated IR radiation better quadratically than linearly. The empirical equations used in this research were able to predict Wangara IR data to within 20-24%.

A modification of Beer's Law was derived to evaluate the residual radiation under clear skies as suggested by Flowers et al. (1969) for SW radiation. With the surface albedo assumed at 0.15, a mean turbidity coefficient of 0.16 was determined. Also, the square root of the optical air mass was found to best represent the data in this equation.

An analysis of SW cloud attenuation coefficients (C-values) from the residual radiation proved inconclusive. A C-value of 0.74 for low clouds at high solar angles was found to be in the range of previously published values (Kondratyev, 1965); C-values at low sun angles and for a combination of middle and high clouds were unrealistically high.

Of considerable importance is the finding that cloud attenuation of the residual radiation behaved nonlinearly. Whereas solutions as high as the fourth order fit the data at noon, quadratic solutions fit well near sunset and sunrise. Overall, relative deviations during the day of the combined parameterization were approximately 20% at noon and just less than 30% for periods up to one hour before sunset or sunrise. Predictions within these one-hour periods, however, contained considerable error, partially due to the scatter and small magnitude of the measurements.

Diurnal trends in surface radiation and other meteorological parameters were established. Comparisons between surface radiation and the other three surface energy fluxes (sensible, latent, and ground heat fluxes) were completed for a mean diurnal trend and under variations of clouds and wind speeds. A good correlation was illustrated for radiation and ground flux.

It is believed that from this work a better understanding has been achieved for the characteristics of the surface radiation budget under small-scale changes in the weather.

Roger T. Edson
Atmospheric Science Department
Colorado State University
Fort Collins, Colorado
Summer, 1980

ACKNOWLEDGMENTS

The author would like to thank the members of his committee, Drs. Robert N. Meroney, Thomas B. McKee, Teizi Henmi and his advisor, Dr. Elmar R. Reiter for their assistance in the preparation of this paper. He would also like to thank Bonnie Grantham who typed the manuscript, Scott Ryden and Mark Howes who aided in the drafting, and Duayne Barnhart for his photographic assistance. Dr. James W. Deardorff of the National Center for Atmospheric Research (NCAR) furnished the magnetic tape for the Wangara data.

The author would especially like to thank Dr. Teizi Henmi for his continuous encouragement and help throughout the time of this research effort.

This research was sponsored by funds from the U.S. Environmental Protection Agency under Grant No. R803685-01 and the National Science Foundation under Grant No. ATM78-17835. Additional computer time was furnished by NCAR. NCAR is supported by the Atmospheric Science Division of the National Science Foundation.

TABLE OF CONTENTS

	<u>Page</u>
1. Introduction	1
2. The Wangara Data	4
3. Theory and Procedure	10
3.1 IR Radiation	10
A. IR Radiation Leaving the Ground	10
B. Obtaining Net IR Radiation Under Cloudless Skies	11
C. Net IR Radiation with Clouds	15
3.2 SW Radiation	18
A. Turbidity	18
B. Surface Albedo	20
C. Cloud Effect Upon Net SW Radiation	22
4. Diurnal Characteristics of Meteorological Conditions and Energy Parameters for the Wangara Experiment	28
4.1 Meteorological Characteristics of the Data	28
A. Data and Cloud Frequency	29
B. Surface Characteristics	33
4.2 Surface Energy Parameters	38
A. Diurnal Characteristics	38
B. Fluctuations in the Energy Parameters	41
4.3 Chapter Summary	47
5. Results: Analysis of Net Radiation for the Wangara Experiment	49
5.1 General Cloud Effects on Net Radiation	49
5.2 IR Radiation	49
A. Net IR Radiation under Clear Skies	49

Table of Contents (Continued)

	<u>Page</u>
B. Cloud Effects on IR Radiation	53
C. Accuracy of the IR Parameterization	61
D. Summary	62
5.3 Residual Radiation	63
A. Residual Radiation under Clear Skies	63
B. Cloud Effects on Residual Radiation	66
C. Accuracy of the Net Radiation Parameterization During the Daytime	70
D. Summary	77
6: Conclusion	79
References	82
Appendix: Sensible Heat Flux Calculation	86
I. Equations	86
II. Procedure	88

LIST OF TABLES

<u>Table</u>	<u>Page</u>
3.1.1 Infrared Emissivities	12
3.1.2 Values of Constants in Brunt Equation	14
3.1.3 Empirical Coefficients Characterizing the Influence of Cloud Cover on Net IR Radiation	16
3.2.1 Albedos for SW Radiation	21
3.2.2 Relative Decrease (in Percent) of the Flux of Total Radiation for the Case of a Continuous Cloud Cover of Different Types and Different Solar Altitudes in Com- parison With the Corresponding Values for a Cloudless Sky	26
4.1.1 Sunrise and Sunset at Hay, Australia	28
5.2.1 Average Nighttime K-Values for Wangara Data	54
5.2.2 Accuracy of Net IR Radiation Equations ($ly\ min^{-1}$)	61
5.3.1 C-Values for Residual Radiation	69
5.3.2 Standard Deviation of Daytime Net Radiation Equations ($ly\ min^{-1}$) and Value of (m)	76
A-1 Initial Values of L (m)	88

LIST OF FIGURES

<u>Figure</u>		<u>Page</u>
2.1	The geography of the Wangara Experiment	5
2.2	The Wangara data display	7
3.2.1	Albedo measurements: Beam reflector versus inverted Eppley	23
3.2.2	Dependence of the reflection, transmission, and absorp- tion of solar radiation upon cloud amount	25
4.1.1	Data size and cloud frequency	30
4.1.2	Mean cloud coverage during the Wangara Experiment . . .	31
4.1.3	Broken cloud coverage during the Wangara Experiment . .	32
4.1.4	Surface temperature and inversion characteristics . . .	34
4.1.5	Wind speed and mixing ratio	37
4.2.1a,b	(a) Net radiation and ground flux, (b) sensible heat and latent heat flux	39
4.2.2a-d	Surface temperature, net radiation, ground flux and sensible heat flux relative deviations	43
5.1	Influence of clouds upon Wangara radiation data	50
5.2.1	Effective radiation under clear skies	52
5.2.2a-d	Cloud amount versus IR radiation	55
5.2.3a,b	(a) Middle clouds versus IR radiation, (b) high clouds versus IR radiation	58
5.3.1	Residual radiation at Hay, Australia	64
5.3.2	Residual radiation under clear and cloudy skies as an approximation for net SW radiation	68
5.3.3a-e	Cloud amount versus residual radiation	71

LIST OF SYMBOLS

$a, b =$	empirical constants in Brunt Equation
$A_{r,c} =$	total SW radiation attenuation
$B =$	turbidity coefficient
$C, C_{Tot}, C_{lo},$ $C_{mi}, C_{hi},$ $C_{no lo} =$	(C-values) SW cloud attenuation coefficients
$c_p =$	specific heat of air at constant pressure
$d, \bar{d} =$	instantaneous and mean distance of the earth from the sun
$e =$	screen height vapor pressure
$F =$	IR radiation flux
$F_o, F_{o,n} =$	effective radiation under clear skies and with clouds (measured at screen height)
$F'_o =$	effective radiation under clear skies (measured at the ground)
$g =$	acceleration due to gravity
$H_o =$	sensible heat flux
$k =$	von Karmen constant
K, K_{Tot}, K_{lo} $K_{mi}, K_{hi},$ $K_{no lo} =$	(K-values) IR cloud attenuation coefficients
$L =$	Monin-Obukov length
$m =$	empirical constant in IR and SW cloud attenuation equa- tions
$M =$	optical air mass
$n, n_{lo}, n_{mi},$ $n_{hi}, n_{no lo} =$	cloud coverage
$Q_s, Q_{go} =$	SW radiation at the top of atmosphere and at the ground
$\bar{Q}_n =$	mean residual radiation at the ground

List of Symbols (Continued)

$Q'_{go}, Q_{g,n}$	=	net SW radiation at ground under clear skies and with clouds
s	=	empirical constant in turbidity equation
S	=	solar constant
T, T_s	=	surface temperature measured at screen height and at the ground
U_m	=	wind speed at height m
u_*	=	friction velocity
x	=	total turbidity coefficient ($\tau_r + \tau_z + B$)
X	=	$(1 - 15\xi)^{\frac{1}{4}}$
Y	=	$(1 - 9\xi)^{\frac{1}{2}}$
z	=	vertical coordinate
z_0	=	roughness height
Z	=	zenith angle
α	=	surface albedo
ϵ	=	IR emissivity
θ, θ_0	=	temperature and surface temperature
θ_*	=	scaling temperature
ξ	=	Z/L
π	=	3.14159 ...
ρ	=	air density
σ	=	Stefan-Boltzman constant
τ_r, τ_z	=	atmospheric scattering and absorption coefficient
$\phi_h(z/L),$ $\phi_m(z/L)$	=	nondimensional temperature and wind
ψ_h, ψ_m	=	stability function for temperature and wind

1. INTRODUCTION

In recent years theoretical advances in the field of meteorology have become increasingly dependent upon a reliable parameterization of the planetary boundary layer. The relationships and feedback mechanisms between events in the boundary layer and upper atmosphere are important to investigations in such fields as climatic modelling and numerical weather prediction. It is therefore an essential task for meteorologist to develop methods that can easily and accurately predict some of the more important meteorological characteristics of the earth's lower atmosphere.

An accurate description of the variability of the surface radiation budget is one such task. Although numerous empirical formulas have been developed to describe the radiation budget on a seasonal basis (Houghton, 1954; Budyko, 1958; London and Sasamori, 1971; Vonder Haar and Suomi, 1971) and on a daily basis (Halstead et al., 1957; Geiger, 1959; Kondratyev, 1965 and Berlyand, 1970), a convenient method to predict radiative flux over a particular observation site on a much smaller time frame such as one hour or less is still sought. Abrupt changes in weather conditions at this scale (such as an increase in cloudiness or a frontal passage) are difficult to model. These changes, however, can significantly alter the balance of energy at the earth's surface. This in turn can influence other meteorological characteristics of the boundary layer such as the sensible heat flux at the ground and the distribution of temperatures in the soil and lower atmosphere, as well as the interaction between the boundary layer and the upper atmosphere.

In order to make such a detailed radiation study, a reliable data set is needed: one with high enough resolution in both time and space to distinguish microscale changes; also, one long enough to represent synoptic scale changes. The 44-day Wangara Experiment (Clark et al., 1971) offers this unique opportunity. Recently, Wangara data have served as references for a number of numerical models of the planetary boundary layer (e.g.; Clark and Hess, 1973; Deardorff, 1974; Pielke and Mahrer, 1975 and Yamada and Mellor, 1975). Several of these models included simple parameterizations of the surface radiation and energy budgets under "ideal" conditions (clear skies and little temperature advection). However, little has been achieved in this aspect under nonideal conditions.

It is the intent of this research to use the Wangara data set to parameterize the surface radiation budget under the influence of changing weather conditions. Previously derived equations and their solutions will be examined and adapted for use for the Wangara data. In particular, those equations which can be easily evaluated from measurements taken by a surface observer will be studied. In this manner, it is hoped that certain characteristics of the boundary layer can be predicted or analyzed near to "real time" without the use of complicated instrumentation or costly investigations. In addition, relationships between surface radiation and several other meteorological parameters in the surface energy budget will be examined.

After a detailed discussion of the Wangara data set in Chapter 2, Chapter 3 will present the procedures and equations to be used. Equations that are investigated include the Brunt equation for infrared (IR)

radiation and a modification of Beer's Law for short wave¹ (SW) radiation under clear skies. Cloud attenuation equations for both IR and SW radiation used by Kondratyev (1965) and others are also presented.

Diurnal profiles of both net radiation and other surface related meteorological parameters are illustrated in Chapter 4. Correlations are determined under different cloud and wind conditions for several of these profiles.

Finally in Chapter 5, the results of the parameterization are presented. A special emphasis is placed both quantitatively and qualitatively on the effect clouds have on net surface radiation.

It is believed that from this work a better understanding has been achieved for the characteristics of the surface radiation budget under small-scale changes.

¹Although SW radiation was not measured directly in this data set, the residual of the IR radiation parameterization subtracted from the net radiation measurements will be studied. This residual radiation will be assumed to approximate net SW radiation to within the accuracy of the daytime IR parameterization.

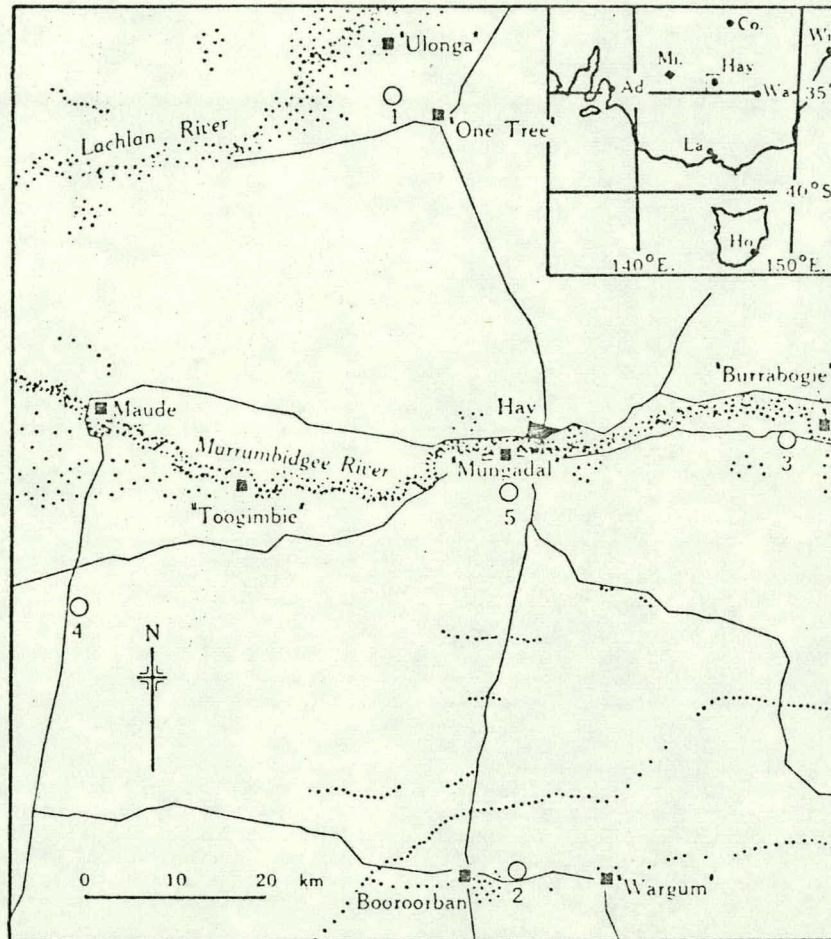
2. THE WANGARA DATA

The data set used in this research is described by Clark et al. (1971) and is known as the Wangara Experiment. Hourly data were collected in southeast Australia near the town of Hay ($34^{\circ}30'S$, $144^{\circ}56'E$) during the Australian winter from 15 July to 27 August 1967.

One of the purposes of the Wangara Experiment was to establish an extensive set of synoptic and micrometeorological data to aid in the understanding of the many complex characteristics of the earth's boundary layer (the lower two kilometers). The voluminous collection of radiation data makes this work particularly attractive for the present research. The Wangara Experiment and the Great Plains expedition of 1953 (O'Neill Experiment) by Lettau and Davidson (1957) contain the best known set of reliable boundary layer data that exist today.

The site for the experiment was chosen because of the relatively large area of flat land with low vegetative cover. Save for a line of eucalyptus along a passing river, the predominant growth consisted of very sparse grass and legumes. The dominant soils in the area were brown loams, 5-20 cm thick, overlying red-brown clay subsoils. Except for brief periods after rain storms, the soils generally were very dry.

To obtain an accurate account of the lower wind field, hourly pilot balloons were released from each of five stations. Four of these stations were located at the corners of a square approximately 60 km on a side with one station in the middle. Their relative location and their elevation is shown in Fig. 2.1. Hay's location in southeast Australia is shown in the inset.



—Location of the five sites, showing the two rivers. The distribution of trees is represented schematically by dots. Townships, station homesteads, and roads are also shown. Coordinates of the five sites from the township of Hay (X , positive eastward; Y , northward) and mean height above sea level, z are as follows:

Station	X (km)	Y (km)	z (m)
1	-20.17	41.61	86.9
2	-4.98	-47.33	88.1
3	27.13	0.70	100.6
4	-51.53	-16.74	78.9
5	-4.52	-5.91	97.8

Inset is a map of the distribution of Bureau stations with twice daily temperature and 6-hourly wind soundings. [Circles indicate both; the symbol at Mi (Mildura) indicates wind soundings only.] The area covered by the detailed map is shown as a square on the inset map. The coordinates of places in the inset map are given on p. 11.

[From Clark et al., 1971.]

Fig. 2.1 The geography of the Wangara Experiment.

An average wind profile was determined for the five stations at 50-meter intervals up to one kilometer, and at 100-meter intervals up to two kilometers. Vector deviations of $5-10 \text{ cm sec}^{-1}$ were computed for moderate winds ($10-20 \text{ m sec}^{-1}$) up to one kilometer in height. When observations from more than three stations were reported, vertical velocities were computed from the continuity equation. Probable error was determined to be approximately $\pm 2 \text{ cm sec}^{-1}$ at the height of one kilometer in moderate winds. In addition to the wind measurements, hourly surface measurements of pressure, wet and dry bulb temperature, "weather", cloud type and amount, and surface wind direction were made at each of the stations. These measurements were averaged and were recorded as single quantities with "weather" determined in a priority system from the International Weather Code.

A sample of the data format is shown in Fig. 2.2. The data are stored in a similar form on magnetic tape.¹ Data are organized in three-hour blocks. Days are numbered consecutively during the extent of the experiment and times are local standard times. Winds are measured in centimeters per second, temperature in degrees centigrade, cloud amounts in oktas, and radiation and heat flux in milliwatts per square centimeter.

Radiosondes launched from the center station measured temperatures and humidity at three-hour intervals. These data were interpolated at the same heights as were the wind profiles. Field measurements from the radiosondes could account for errors up to 0.4°C . Humidity measurements

¹ Magnetic tape was obtained from Dr. J.W. Deardorff at NCAR, Boulder, CO.

	DAY 8 TIME 2004 E.S.T.	DAY 8 TIME 2103 E.S.T.	DAY 8 TIME 2200 E.S.T.	DATA PAGE 63
	PRESSURE 1012.3 MB.	PRESSURE 1012.7 MB.	PRESSURE 1013.0 MB.	TIME 2100 E.S.T.
SCREEN	TEMP 11.7 C. WET BULB 9.5 C.	TEMP 10.9 C. WET BULB 9.1 C.	TEMP 10.6 C. WET BULB 8.9 C.	GEOSTROPHIC WIND FROM SYNOPTIC NETWORK U 231 418 CH/M S
WEATHER	LOW 7.0 TOTAL 7.0 SC	LOW 7.4 TOTAL 7.4 CB	LOW 7.6 TOTAL 7.6 CB	THERMAL WIND U V 0-1 KM 147 -98 CH/M S
CLOUD DKT.				1-2 KM 143 111
HEAT FLUX MW/50.CM	H ***** R -2.1 G -0.8	H ***** P -3.3 G -1.4	H ***** P -1.6 G -0.8	RADIO-SOUNDING
	WIND DIRECTION 259 DEG	WIND DIRECTION 249 DEG	WIND DIRECTION 240 DEG	DAY 8 TIME 2106 E.S.T.
	STATION 5 STATION 4	STATION 5 STATION 4	STATION 5 STATION 4	WT. PRESS. TEMP. MIXING RATIO
U 0.5 M	182 CM/S ***** CM/S	129 CM/S ***** CM/S	106 CM/S ***** CM/S	M. MB. C. G/KG
U 1	206 160	149 109	119 72	SURF 1013 10.9 6.2
U 2	230 198	174 136	142 102	50 1007 12.1 6.8
U 4	257 242	215 174	174 139	100 1001 11.8 6.7
U 8	299 296	279 220	222 182	495 11.5 6.6
U 16	354 385	367 229	280 240	200 989 11.2 6.5
DT 2-1 M	0.17 C.	0.23 C.	0.23 C.	300 983 10.9 6.4
DT 4-2	***** C.	***** C.	U.14 C.	400 977 10.6 6.3
HEIGHT M	U V W N	U V W N	U V W N	400 971 10.3 6.3
50	436 130 -0.0 5	395 167 0.1 5	290 206 0.1 5	400 966 10.0 6.2
100	504 181 -0.1 5	462 238 0.1 5	351 275 0.0 5	500 954 9.2 6.0
	519 251 -0.3 5	452 309 0.0 5	371 323 0.0 5	600 948 8.8 5.8
200	516 315 -0.7 5	437 364 -0.1 5	360 355 -0.0 5	600 943 8.3 5.7
	507 326 -1.1 5	443 393 -0.2 5	368 394 -0.1 5	700 937 7.8 5.6
300	550 358 -1.5 5	451 426 -0.3 5	366 412 -0.1 5	700 931 7.3 5.4
	505 359 -1.8 5	456 454 -0.4 5	384 412 -0.1 5	800 926 6.9 5.3
400	547 425 -2.1 5	395 433 -0.6 5	358 411 -0.2 5	800 920 6.5 5.2
	527 451 -2.4 5	440 473 -0.7 5	365 420 -0.3 5	900 914 6.2 5.1
500	519 460 -2.5 5	462 501 -0.7 5	383 435 -0.3 5	900 909 5.8 5.0
	531 527 -2.7 5	441 510 -0.7 5	384 450 -0.4 5	1000 903 5.4 4.9
600	534 550 -2.7 5	429 504 -0.7 5	404 482 -0.5 5	1000 898 5.0 4.8
	503 518 -2.8 5	430 500 -0.7 5	417 495 -0.5 5	
700	497 496 -2.8 5	434 502 -0.8 5	427 503 -0.5 5	1100 887 4.2 4.7
	515 491 -2.8 5	422 525 -0.9 5	439 529 -0.5 5	1200 876 3.2 4.5
800	518 497 -2.9 5	421 529 -1.1 5	445 577 -0.4 5	1200 865 2.3 4.4
	543 470 -3.0 5	451 540 -1.2 5	447 602 -0.4 5	1400 865 1.3 4.2
900	562 463 -3.0 5	455 562 -1.4 5	453 608 -0.3 5	1600 844 0.4 4.1
	540 423 -3.0 5	459 565 -1.4 5	440 591 -0.3 5	1600 834 -0.1 3.9
1000	538 408 -3.0 5	457 561 -1.4 5	432 575 -0.3 5	1800 823 -0.4 3.8
				1800 813 0.8 3.9
1100	478 440 -3.0 5	465 524 -1.3 5	374 577 -0.2 4	2000 803 1.5 3.6
				2000 793 1.5 2.7
1200	546 459 -2.7 5	444 528 -1.2 4	375 567 0.1 4	
	440 388 -2.3 5	377 528 -1.1 3	362 544 0.4 4	
1400	490 339 -1.7 4	278 527 ***** 2	333 230 ***** 1	
	499 349 -1.4 3	***** ***** 0	321 298 ***** 1	
1600	633 104 ***** 1	***** ***** 0	***** ***** 0	
	699 362 ***** 1	***** ***** 0	***** ***** 0	
1800	667 65 ***** 1	***** ***** 0	***** ***** 0	
	636 60 ***** 1	***** ***** 0	***** ***** 0	
2000	677 75 ***** 1	***** ***** 0	***** ***** 0	
GEOS.	333 355 ***** 1	170 26 ***** 0	258 40 ***** 0	
500M.ACC. CH/S.50	-0.003 -0.002	-0.016 -0.009	-0.013 -0.005	

Fig. 2.2 The Wangara data display. [From Clark et al., 1971.]

were accurate within 5%, and large discrepancies between surface and radiosonde measurements were so noted in the report.

In order to estimate heat and momentum fluxes near the ground, an extensive micrometeorological program was maintained at two of the stations (Station 5 was primarily used and Station 4 was used as a backup). Wind speeds were measured at 0.5, 1, 2, 4, 8 and 16 m. The temperature differences between 1 and 2, and 2 and 4 m were also obtained. A Funk radiometer (Funk, 1959; or see Sellers, 1974, p. 79) was used to measure net radiation near the ground and three flux plates placed just below the surface were utilized to obtain values of ground heat flux. In addition, for five days, a fluxatron (Dyer et al., 1967) directly measured daytime heat flux. All micrometeorological measurements were recorded hourly and were based on half-hour averages, centered on the hour.

Finally, geostrophic and thermal winds were estimated from six stations in eastern Australia as well as from the Wangara network (see Fig. 2.1).

The time of year and location of the Wangara Experiment were chosen to study the boundary layer under a variety of synoptic conditions. During this period, midlevel westerlies were prevalent, and cold fronts crossed over the site every three or four days. Rainfall was generally quite light over the entire period with a total accumulation of approximately 26 mm spread over seven days (one day reported 14 mm).

In conclusion, the Wangara data set provides a wealth of information to aid in the study of the earth's surface radiation budget. Its hourly resolution and data collection network is sufficient to cover

most small-scale effects while its length is long enough to last through several synoptic scale changes in the weather.

3. THEORY AND PROCEDURE

Empirical equations are cited in the literature that predict surface radiative flux over a season as well as on a daily basis. It is the purpose of this chapter to present several of these equations and their associated coefficients in a form suitable for parameterization and comparison to the higher resolution Wangara data.

Net radiative flux is normally determined by equations describing IR and SW radiation individually. Since net IR radiation can be taken directly from the nocturnal Wangara radiation data, it will be investigated initially. Once an adequate procedure to simulate the IR flux is found, a residual can be determined from the net radiation measurements during the daytime in order to approximate net SW radiation. A procedure can then be found to approximate this residual radiation.

3.1 IR Radiation

A. IR Radiation Leaving the Ground

The laws of thermodynamics state that a body that absorbs energy will then radiate energy at an uniform temperature particular to the physical properties of that body. The earth absorbs SW radiation from the sun and radiates IR radiation at an equilibrium temperature which is usually close to that of the surface temperature. The Stefan-Boltzman Law describes this process:

$$\text{IR Flux} = F = \epsilon \sigma T_s^4 \quad 3.1.1$$

where ϵ is the emissivity, σ the Stefan-Boltzman constant, and T_s the surface temperature. If the IR flux is given in langley's per minute (ly min^{-1}), then temperature is given in Kelvin (K) and σ equals $8.14 \times 10^{-11} \text{ ly min}^{-1} \text{ K}^{-4}$. For a perfect radiator, a black body, ϵ is 1.0, but

for other than a perfect radiator, such as the earth's surface, ϵ is less than 1.0. Table 3.1.1 compiled by Sellers (1974) shows IR emissivity for various ground conditions found on the earth. Other works by Geiger (1959), Buettner and Kern (1965), Griggs (1968) and Fuchs and Tanner (1968) further support this data. With the aid of Table 3.1.1, it has been approximated for this research that the dry, sandy, grassland conditions at Hay, Australia radiates with an emissivity of 0.9.

B. Obtaining Net IR Radiation Under Cloudless Skies.

The earth's atmosphere and its constituents behave radiatively in a manner similar to that of its surface. Radiation emanating from both the sun and the earth is absorbed in the atmosphere. Energy is in turn radiated in all directions, including back to the earth (counter-radiation). The difference of the flux of IR radiation leaving the surface (Eq. 3.1.1) and the flux of counter-radiation returning to the surface is defined as net IR radiation.

One objective of this research is to establish an equation to determine IR radiation that can be easily evaluated from surface observations using standard meteorological instrumentation. Several studies have substantiated the possibility of such an equation. Brunt (1932) and Geiger (1959) described experiments showing a high correlation between net IR radiation and near surface (1-2 m) air temperature and moisture measurements. These studies were further verified by Sellers (1974, p. 46). He found that most of the counterradiation reaching the ground during the O'Neill experiment came from the earth's lowest 100-meters (58.9% of the total counterradiation originated from below 100-meters height and 25.8% from below 2-meters height).

Table 3.1.1

INFRARED EMISSIVITIES
(Percent)

<i>A. Water and Soil Surfaces</i>		<i>C. Vegetation</i>	
Water.....	92-96	Alfalfa, dark green.....	95
Snow, fresh fallen.....	82-99.5	Oak leaves.....	91-95
Snow, ice granules.....	89	Leaves and plants.....	
Ice.....	96	0.8 μ	5-53
Soil; frozen.....	93-94	1.0 μ	5-60
Sand, dry playa.....	84	2.4 μ	70-97
Sand, dry light.....	89-90	10.0 μ	97-98
Sand, wet.....	95		
Gravel, coarse.....	91-92	<i>D. Miscellaneous</i>	
Limestone, light gray....	91-92	Paper, white.....	89-95
Concrete, dry.....	71-88	Glass pane.....	87-94
Ground, moist, bare....	95-98	Bricks, red.....	92
Ground, dry plowed....	90	Plaster, white.....	91
		Wood, planed oak.....	90
<i>B. Natural Surfaces</i>		Paint, white.....	91-95
Desert.....	90-91	Paint, black.....	88-95
Grass, high dry.....	90	Paint, aluminum.....	43-55
Fields and shrubs.....	90	Aluminum foil.....	1-5
Oak woodland.....	90	Iron, galvanized.....	13-28
Pine forest.....	90	Silver, highly polished...	2
		Skin, human.....	95

[From Sellers, 1974]

Two equations that describe net IR radiation under clear skies and require only the specification of surface parameters to be evaluated are Angström's Equation and derived from it the Brunt Equation (Brunt, 1932). The more widely used Brunt Equation is examined in this research and can be written:

$$F_0 = \epsilon\sigma T^4(a - b\sqrt{e}) \quad 3.1.2$$

where F_0 is the net IR radiation with no clouds and a and b are empirical constants. The air temperature, T , and vapor pressure, e , (measured in millimeters of mercury [mmHg]) are observed at screen height (which for the Wangara data is 1.2 m).¹ Values of the constants a and b are readily available in the literature and have been compiled in surveys by Geiger (1959), Kondratyev (1965), Berlyand (1970) and Sellers (1974). Table 3.1.2 contains a list of these values. These values can be compared to those estimated from the Wangara data.

With a and b evaluated, Eq. 3.1.2 can be then used under any sky condition in conjunction with the proper modification for cloud cover.

¹ The use of the screen height temperature, T , is adequate in this equation if there is not a large difference between T and the actual surface temperature, T_s . However, a significant gradient between the two heights could result in an unreasonable representation of the true upward flux. Budyko (1958) and others have suggested a correction to the above equation as follows:

$$F'_0 = F_0 + 4\epsilon\sigma T^3(T_s - T).$$

This modification is not used in this research because of the difficulty in obtaining a true surface temperature. Also, a gradient as large as 5°C at a screen height temperature of 0°C would only amount to an IR correction of .03 ly min⁻¹. This is probably within the accuracy of the Brunt Equation.

Table 3.1.2 Values of Constants in Brunt Equation.

a	b	Year	Author
.75, .45	.065, .056	1932, 1940	Brunt
.42	.051	1933	Angström
.53	.061	1935	Ramanthan and Desai
.448	.064	1946	Lyutershteyn and Chudnovskiy
.376	.043	1947	Chumakova
.39	.058	1952	M. Ye. Berlyand and T.G. Berlyand
.39	.050	1956	Budyko
.355	.055	1957	DeCoster and Shuepp
.34	.039	1957	Goss and Brooks
.305-.395	.040-.078	1961	Marshunova
.47	.065	1961	Monteith

C. Net IR Radiation with Clouds.

It is generally recognized that cloud cover influences net IR radiation. For example, it is observed that cloudy nights are much warmer than nights with clear skies; this is because the clouds radiate downward at a temperature close to that of their base and therefore increase the counterradiation of the sky.

This phenomenon is described by a formula that has been used frequently by researchers (Halstead et al., 1957; Philip, 1957; Geiger, 1959; Kondratyev, 1965; Adem, 1967; Berlyand, 1970 and Kumor, 1978):

$$F_{o,n} = F_o(1 - Kn^m) \quad 3.1.3$$

where $F_{o,n}$ is the net IR radiation with clouds, K and m are empirical constants, and n is the amount of cloudiness in tenths. Values of m have ranged between 1.0 and 2.7 with 1.0 and 2.0 being the most common values used (Kondratyev, 1965). (It follows that the higher the value of m , the less scattered (\leq five-tenths) cloud conditions will attenuate radiation.) Values of K are determined by measuring the effect which an overcast sky of a particular cloud type has on the attenuation of net IR radiation. Once F_o is estimated (Eq. 3.1.2), the only remaining observations needed to evaluate Eq. 3.1.3 are the cloud type and amount.

As a variation of the above equation, the coefficient, K , can represent cloud attenuation for individual cloud types (e.g., stratus, cumulus, altocumulus, cirrus, etc.) or for a cloud group (i.e., high, medium or low). Previous investigations have calculated K for the above cloud group, and a summary of the findings found in Kondratyev (1965) is presented in Table 3.1.3. The range found for each K in the individual studies is probably due to the uniqueness of each cloud cover observed

Table 3.1.3 Empirical Coefficients Characterizing the Influence of Cloud Cover on Net IR Radiation.

Author	Station	K_{hi}	K_{mi}	K_{τ_0}
Defant	Stockholm			0.86
Angström	Stockholm			0.90
Akslef	Uppsala	0.20	0.77	0.83
Dorno	Davos	0.31	0.63	0.85
Yefimov	Bukhta Tikhaya	0.20	0.59	0.84
Yefimov	Mys Shmidta	0.20	0.57	0.81
Yefimov	Pavlovsk	0.22	0.52	0.76
Yefimov	Tashkent	0.16	0.50	0.67
Lyutershteyn	Tashkent	0.1; Ci 0.2-0.3 Cs and Cc	0.4; Ac and Ac trans. 0.6; Ac and Ac op.	0.8; St and Ns 0.75-0.85; Cu 0.95-1.0; Cb

(From Kondratyev, 1965)

and to observational technique and location characteristics. In this research, these values are compared to those calculated with the Wangara data.

Under layered conditions, then, K can be given as either a single value effect for all clouds present, K_{Tot} , (Eq. 3.1.3) or as a combination of parts for each different cloud type or group:

$$K_n^m = K_{lo} n_{lo}^m + K_{mi} n_{mi}^m + K_{hi} n_{hi}^m \quad 3.1.4$$

where lo , mi , and hi represent low, middle, and high cloud bases, respectively.

This relationship has had limited verification. One possible problem is the fact that the equation can not distinguish the type of cloud(s) directly overhead. From geometrical considerations, clouds directly overhead probably have more of an effect on the radiation budget than clouds that are off to one side.²

Nevertheless, Eq. 3.1.3 and Eq. 3.1.4 are used in this research to determine the cloud effect on IR radiation. The relative accuracy of both these equations can be tested. In this way the importance of distinguishing individual cloud types, rather than treating the sky cover as a whole, is investigated.

With IR radiation parameterized, a residual can be determined from the daytime net radiation measurements which can be then approximated by empirical equations for net SW radiation.

² The method by which cloudiness was measured in the Wangara data can further enhance this problem, since cloudiness was recorded as an average of several stations rather than as a single observation. However, it is assumed that the cloud conditions were more synoptically than locally affected; therefore, on the average, differences from one station to the next should have been minimal.

3.2 SW Radiation

Net SW radiation can be expressed by:

$$Q_{g,n} = (1 - \alpha)(A_{r,c})(Q_s) \quad 3.2.1$$

where α is the surface albedo, Q_s is the solar radiation incident on a horizontal surface at the top of the atmosphere, and $Q_{g,n}$ is the amount of radiation both direct and scattered, being absorbed by the earth's surface. $A_{r,c}$ is a function of turbidity and cloud attenuation: solar radiation can be scattered back to space or absorbed by clouds as well as be scattered back or absorbed by dry air molecules, dust, ozone and water vapor (Sellers, 1974). The fact that rapid changes in clouds, dust and water vapor can greatly influence SW radiation reaching the ground makes parameterization very difficult, especially since the amount of dust and water vapor present at any one time can not be readily determined from surface measurements. Also, experiments have shown that the surface albedo, α , changes with surface cover, shape and possibly with cloud cover and solar angle.

The Wangara data did not record direct solar radiation separately. Thus, only a residual can be deduced from the measurements. It is assumed that within the limitations of this research's capability to predict IR radiation during the daytime, this residual radiation will adequately approximate net SW radiation. Before equations describing cloud influence on net SW radiation can be studied, a rough estimate of the effect of turbidity and surface albedo must be made.

A. Turbidity

If there are no clouds between the observer and the sun, the intensity of direct solar radiation for a given solar angle depends on the

variable amount of dust, ozone, haze and water vapor in the atmosphere; the extinction produced by these constituents is called atmospheric turbidity.

In order to study turbidity, one must first be able to specify the solar radiation reaching the top of the atmosphere. This is easily described by:

$$Q_s = S(\bar{d}/d)^2 \cos Z \quad 3.2.2$$

where S is the solar constant ($\approx 2.0 \text{ ly min}^{-1}$), $(\bar{d}/d)^2$ represents the square of the ratio of the mean and instantaneous distance of the earth from the sun (0.95 during the Wangara Experiment) and Z is the zenith angle of the sun.

Measurements of turbidity have been recorded by many researchers (e.g.; Kimball, 1919; Wexler, 1934; Robinson, 1962 and Flowers et al., 1969). Since most of these measurements were made for individual stations and techniques and instrumentation have varied with the experiments, comparisons are difficult to make. Flowers et al. analyzed a network of stations throughout the United States for five years. In their report, seasonal and geographical variations in turbidity are described. They noted that the water content of the atmosphere is a significant factor in determining turbidity, and weather conditions that support moist air have higher turbidities.

A modification of Beer's Law has been used by Flowers et al. and others to determine turbidity:

$$Q_{go}/Q_s = 10^{-(\tau_r + \tau_z + B)M} \quad 3.2.3$$

where Q_{go} is the solar radiation reaching the ground, τ_r and τ_z are the scattering coefficient for air molecules and the absorption coefficient

for ozone, respectively. The turbidity coefficient, B , includes both dust and moisture absorption. Under typical conditions in the United States (any season) for optical air mass, M , equal to one³, and at sea level, Flowers et al. approximated $\tau_r = 0.0634$ and $\tau_z = 0.0040$. B was found to range between 0.03 and 0.35.

The adaptability of this equation for general use is apparent. If the values of the extinction coefficients are independently ascertained, knowledge of the solar altitude is all that is required to estimate Q_{go} . In this research values of the turbidity coefficient can be roughly determined from the residual radiation under clear skies. From these estimates the practicality of using a mean single coefficient is investigated.⁴

B. Surface Albedo

When only direct SW radiation is available (and not net radiation as in the Wangara data), the character of the surface albedo must be known in order to calculate the amount of radiation being absorbed by the ground. Surface albedo has been studied with measurements taken from the ground, in airplanes and satellites (e.g.; Fritz, 1948; Houghton, 1954; Kuhn and Suomi, 1958; Bauer and Dutton, 1962 and Vonder Haar and Suomi, 1969). Table 3.2.1 compiled by Sellers (1974) illustrates the variabilities found in the surface albedo from one type of surface to another. As evident from this figure, surfaces such as snow

³ $M \sim \sec Z$ for $z < 80^\circ$

⁴ It should be noted that the above procedure assumes a constant surface albedo with solar altitude (to be discussed next) and that any change in turbidity with cloud cover will be parameterized as a cloud effect.

Table 3.2.1

ALBEDOS FOR THE SHORTWAVE PORTION OF THE
ELECTROMAGNETIC SPECTRUM
(Wavelengths $< 4.0\mu$)

<i>A. Water Surfaces</i>		<i>C. Natural Surfaces (cont.)</i>	
Winter— 0° latitude...	6	Forest, coniferous.....	5-15
30° latitude...	9	Tundra.....	15-20
60° latitude...	21	Crops.....	15-25
Summer— 0° latitude...	6	<i>D. Cloud Overcast</i>	
30° latitude...	6	Cumuliform.....	70-90
60° latitude...	7	Stratus (500-1,000' thick)	59-84
<i>B. Bare Areas and Soils</i>		Altostratus.....	39-59
Snow, fresh fallen.....	75-95	Cirrostratus.....	44-50
Snow, several days old...	40-70	<i>E. Planets</i>	
Ice, sea.....	30-40	Earth.....	34-42
Sand dune, dry.....	35-45	Moon.....	6.7
Sand dune, wet.....	20-30	Jupiter.....	73
Soil, dark.....	5-15	Mars.....	16
Soil, moist gray.....	10-20	Mercury.....	5.6
Soil, dry clay or gray...	20-35	Neptune.....	84
Soil, dry light sand.....	25-45	Pluto.....	14
Concrete, dry.....	17-27	Saturn.....	76
Road, black top.....	5-10	Uranus.....	93
<i>C. Natural Surfaces</i>		Venus.....	76
Desert.....	25-30	<i>F. Human Skin</i>	
Savanna, dry season....	25-30	Blond.....	43-45
Savanna, wet season....	15-20	Brunette.....	35
Chaparral.....	15-20	Dark.....	16-22
Meadows, green.....	10-20		
Forest, deciduous.....	10-20		

[From Sellers, 1974]

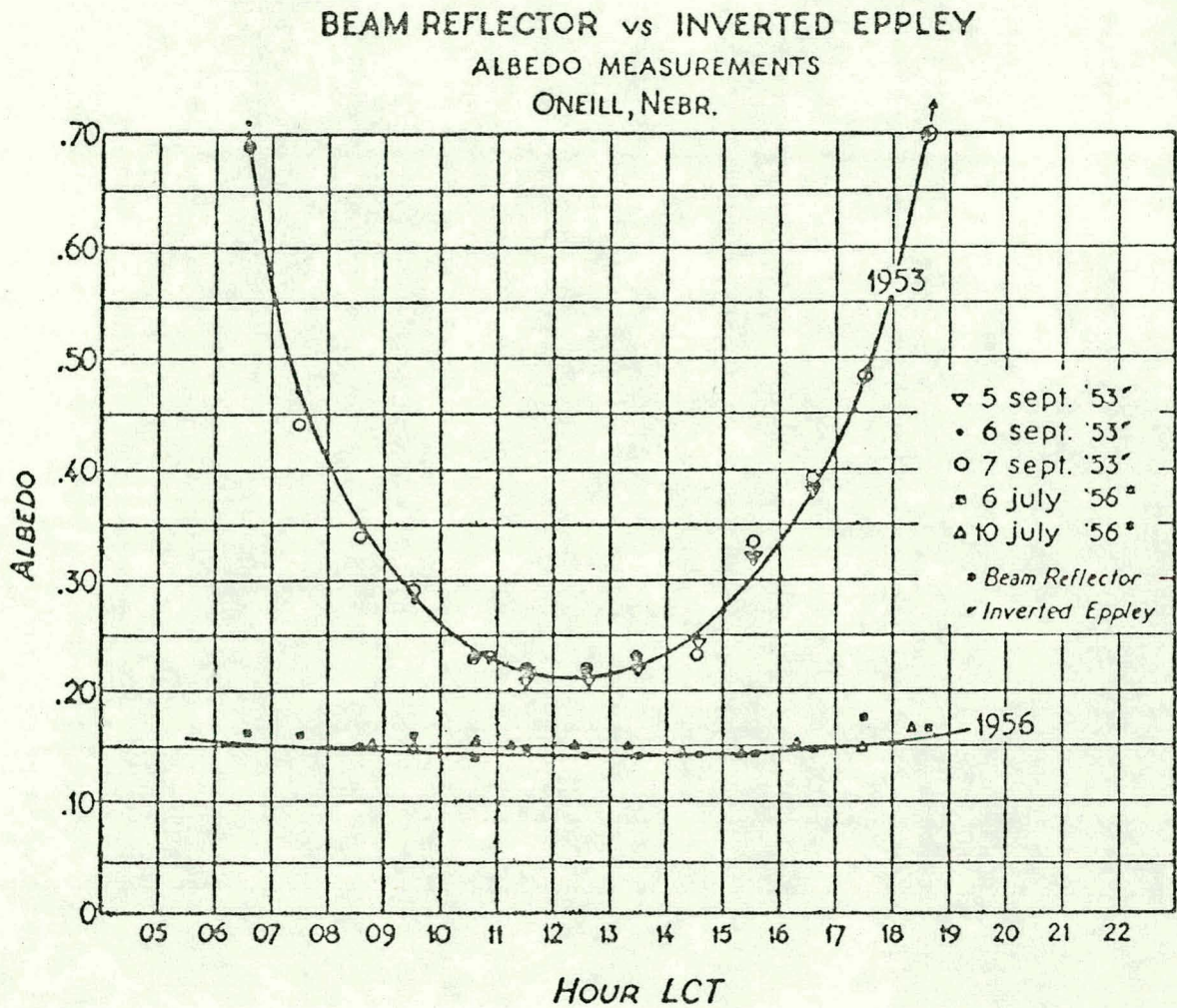
and sand have a considerable effect upon the surface radiation budget. Also it can be seen how wet surfaces cause the albedo to decrease. Fortunately the soil conditions for the Wangara Experiment remained dry during most of the period.

Another possible cause for the albedo to change is the daily motion of the sun. Geiger (1959) and Budyko (1958) presented results that demonstrated greater than 100% changes in albedo between noon and near sunset or sunrise. On the other hand, works by Bauer and Dutton (1962) and Kuhn and Suomi (1958) presented contrary evidence. In fact, Kuhn and Suomi attributed the albedo changes found in the O'Neill data to incorrect interpretations of the instrument (Fig. 3.2.1). Their results show surface albedo remaining fairly constant over a diurnal period. In any case, most studies agreed that an increase in scattered radiation over direct radiation due to increased cloud cover helped alleviate any solar angle effect.

Based on the above evidence and Table 3.2.1, the surface albedo for the Wangara data has been accepted as 0.15. The effect of clouds on SW radiation can now be examined.

C. Cloud Effect Upon Net SW Radiation.

Cloud effects on SW radiation are complicated and difficult to predict. One must explain how much direct and scattered radiation reaches the surface at any particular time under a variety of weather conditions. Clouds are highly variable in their movements, shapes, and sizes; thus, it is hard to make a general prediction of their ability to transmit radiation. Furthermore, a small change in solar angle can strongly enhance or minimize solar attenuation depending upon the location and types of clouds present.



Beam reflector *versus* inverted Eppley
albedo measurements.

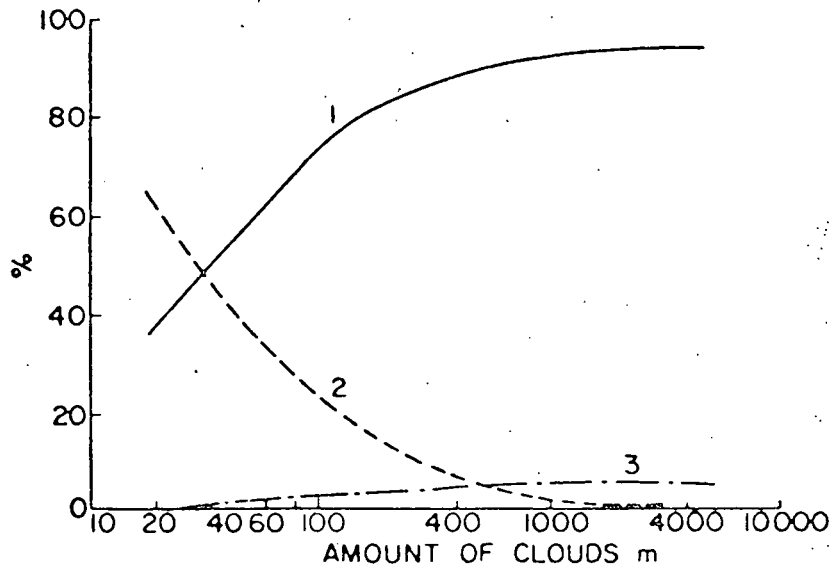
Fig. 3.2.1 Kuhn and Sumoi, 1958, show in their 1956 measurements that diurnal variations in albedo demonstrated in the 1953 O'Neill Experiment were due to incorrect interpretations of the instrument. [From Kuhn and Suomi, 1958.]

Despite these complications, general conclusions can be made concerning cloud attenuation. Obviously, an increase in cloudiness decreases the total solar transmission to the ground. Likewise, a thicker cloud deck reflects and absorbs more radiation. (More radiation is transmitted through thin cirrus than through a cumulonimbus cloud.) Figure 3.2.2 from Hewson (1943) illustrates some of these characteristics.

Table 3.2.2 from Kondratyev (1965) exemplifies how solar angle affects SW attenuation under cloudy skies for different cloud types as compared to cloudless skies. Similar results are found in works by Geiger (1959), Haurwitz (1948), Budyko (1958) and Berlyand (1970). In Budyko's work, cloud attenuation (no cloud type distinction) changed from 50% at a solar altitude of 50° to 78% at an altitude of 5° . Table 3.2.2 indicates that this effect is perhaps most important in cirrus type clouds. In some cases, however, the increase in scattered radiation with lower solar altitude is actually greater than the decrease in direct radiation resulting in an increase in total flux.

This research requires an equation that can describe SW radiation with respect to the sun's position under variable cloud conditions. Ideally, it is desirable to use a method similar to that of Eq. 3.1.3 for IR radiation. In addition to the advantage of being able to compare the two results, this type of equation can be easily put into general application.

Equation 3.2.4, below, meets this criterion and a form of it has been used in surveys by Budyko (1958), Geiger (1959) and Kondratyev (1965):



Dependence of the reflection (1), transmission (2) and absorption (3) of solar radiation upon cloud amount.

Fig. 3.2.2 The effect of cloud thickness upon solar radiation.
[From Hewson, 1943.]

Table 3.2.2 Relative Decrease (in Percent) of the Flux of Total Radiation for the Case of a Continuous Cloud Cover of Different Types and Different Solar Altitudes in Comparison With the Corresponding Values for a Cloudless Sky.

Cloud Type	Solar Altitude, Deg.					
	5	10	20	30	40	50
Ci	44	50	34	22	10	2
Cs	33	39	51	35	20	10
Ac	33	39	46	55	46	38
St fr,	78	83	80	77	77	76
Sc	89	78	68	71	72	73
St	78	78	80	81	83	84

(From Kondratyev, 1965)

$$Q_{g,n} = Q'_{go} (1 - Cn^m)$$

3.2.4

where m is usually equal to 1, Q'_{go} is the net SW radiation absorbed by the ground without clouds, and C is a cloud attenuation coefficient.

Assuming that surface albedo does not change with an increase in cloud cover, values of C should be the same for both absorbed SW radiation (as approximated by the residual radiation in this present study) and SW radiation reaching the ground (usually measured). Under layered conditions, C can be treated (as has been previously done for the IR parameterization) as either a single value effect for all clouds present (C_{Tot}) or as a combination of parts for each different cloud type (C_{l0} , C_{mi} and C_{hi}). Values of the coefficient C can then be compared with attenuations given in Table 3.2.2. Finally, it is of particular interest to see whether there is any variation under different solar angles in the exponent, m , since this indicates the relative importance which an increase in cloudiness can have on the radiation budget.

This chapter has presented the equations needed to parameterize the radiation flux at the earth's surface. With the aid of the hourly Wangara data, the adaptability of these equations for better time resolutions can now be determined.

4. DIURNAL CHARACTERISTICS OF METEOROLOGICAL CONDITIONS AND ENERGY PARAMETERS FOR THE WANGARA EXPERIMENT.

It is necessary to ascertain the mean diurnal influences on the radiation budget before procedures can be taken to predict its changes. In this chapter, diurnal properties of the Wangara data are examined. In particular, hourly composites are made of the parameters needed to evaluate the equations in Chapter 3. Once this is done, the four components of the surface energy budget (net surface radiation, sensible, latent and ground heat flux) can be analyzed for their diurnal trends and for their relationships to each other under different meteorological conditions.

4.1 Meteorological Characteristics of the Data

Perhaps the most important influence in the diurnal trend of surface radiation, as well as in most other meteorological parameters in the lower atmosphere, is the times of sunrise and sunset. Table 4.1.1 gives values for three selected days covering the extent of the Wangara Experiment. Since there is a half-hour difference between Day 1 and Day 44, the times of sunrise and sunset are henceforth given in this research for the middle day, Day 21.

Table 4.1.1 Sunrise and Sunset at Hay, Australia.

	Day 1 15 July	Day 21 5 Aug.	Day 44 27 Aug.
Sunrise	7 ^h 22'	7 ^h 8'	6 ^h 50'
Sunset	17 ^h 26'	17 ^h 40'	17 ^h 58'

In the majority of figures to follow, the graphs are constructed so that the abscissa exhibits nighttime hours in the center. This enables the effect of sunrise and sunset to be more easily demonstrated.

A. Data and Cloud Frequency

Figure 4.1.1 presents hourly radiation data and cloud frequency statistics. The top curve illustrates the number of days for each hour on which radiation data existed. During these periods, averages and profiles were made for the meteorological parameters presented in this paper. As indicated by the graph, most hourly averages calculated were based on over 36 sample measurements.¹

In order to test the effect which clouds of different heights had on the radiation budget, the data were divided into three cloud categories: Total Clouds, Only Low Clouds, and No Low Clouds. The three lower curves in Fig. 4.1.1 indicate the diurnal frequency of each category. When clouds of any type or amount were reported, data were included in the Total Clouds category. Data were included in the Only Low Clouds category when low clouds (Cb, Cu, Ns, St and Sc) made up at least 85% of the reported coverage. Data were included in the No Low Clouds category (As, Ac, Ci, Cs and Cc) when no more than 15% of the sky included low clouds. Separate categories were not made for middle and high clouds because the Wangara data did not quantify these two cloud types separately.

Diurnal cloud coverage is further illustrated in Figs. 4.1.2 and 4.1.3. In these figures, mean cloudiness and the frequency of broken cloud coverage for both low clouds and total sky coverage are given.

¹ A majority of the missing data are accounted for by a four-day rest break in the middle of the experiment.

DATA SIZE AND CLOUD FREQUENCY

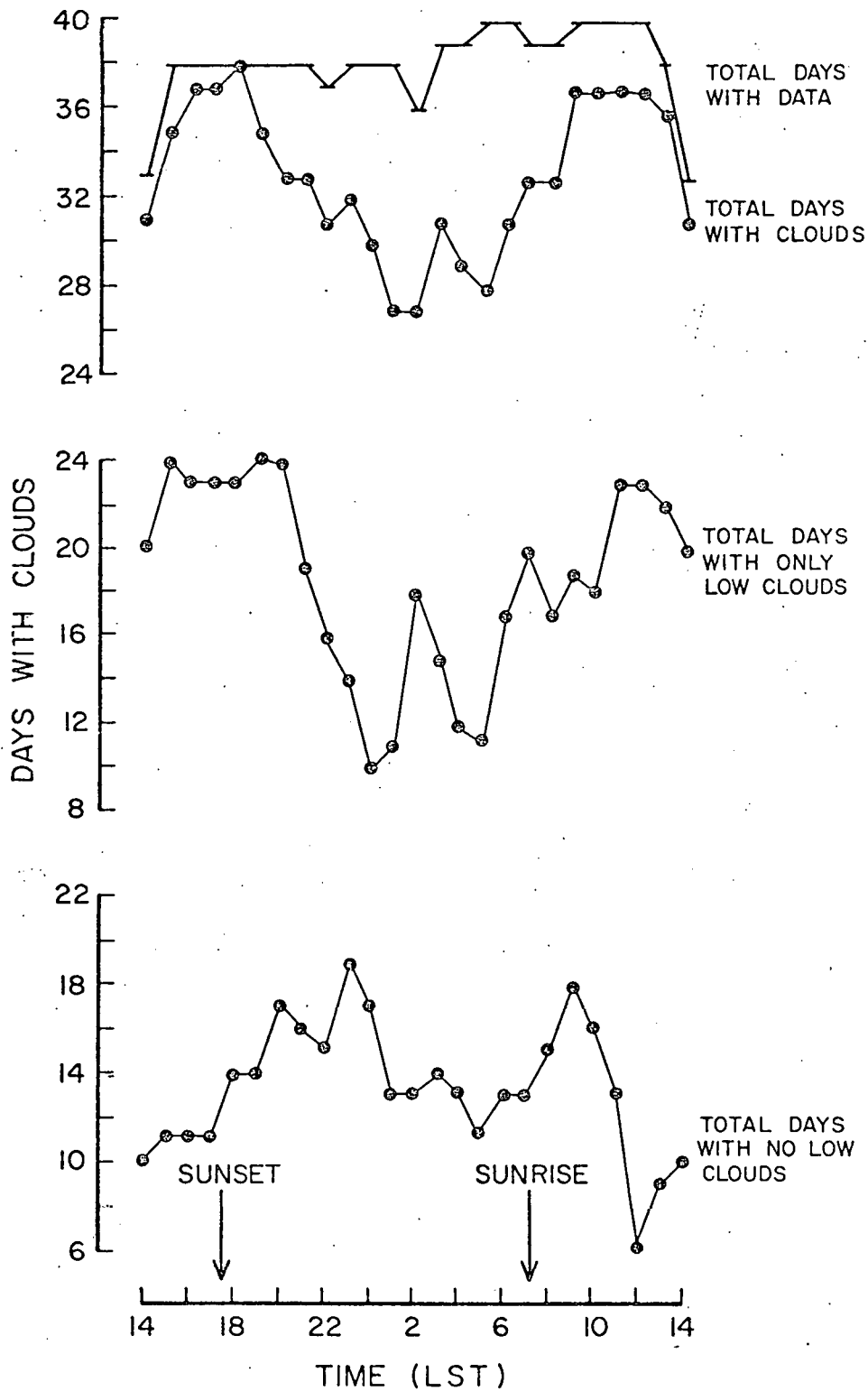


Fig. 4.1.1 Diurnal characteristics of cloud coverage (any amount) for the Wangara Experiment. Top curve represents number of days that radiation data was received.

MEAN CLOUD COVERAGE DURING WANGARA EXPERIMENT

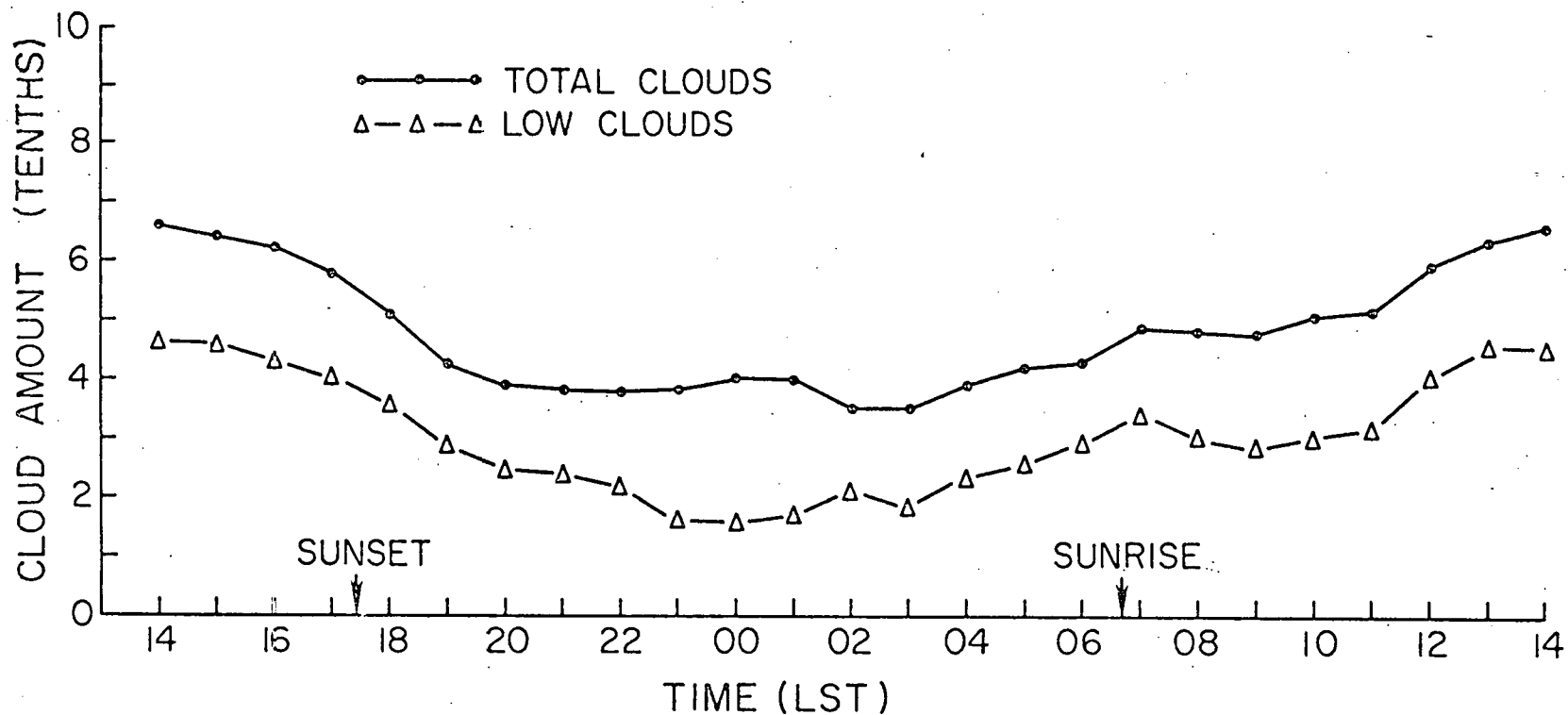


Fig. 4.1.2 Mean cloudiness for total clouds and low clouds during the Wangara Experiment.

BROKEN CLOUD COVERAGE DURING WANGARA EXPERIMENT

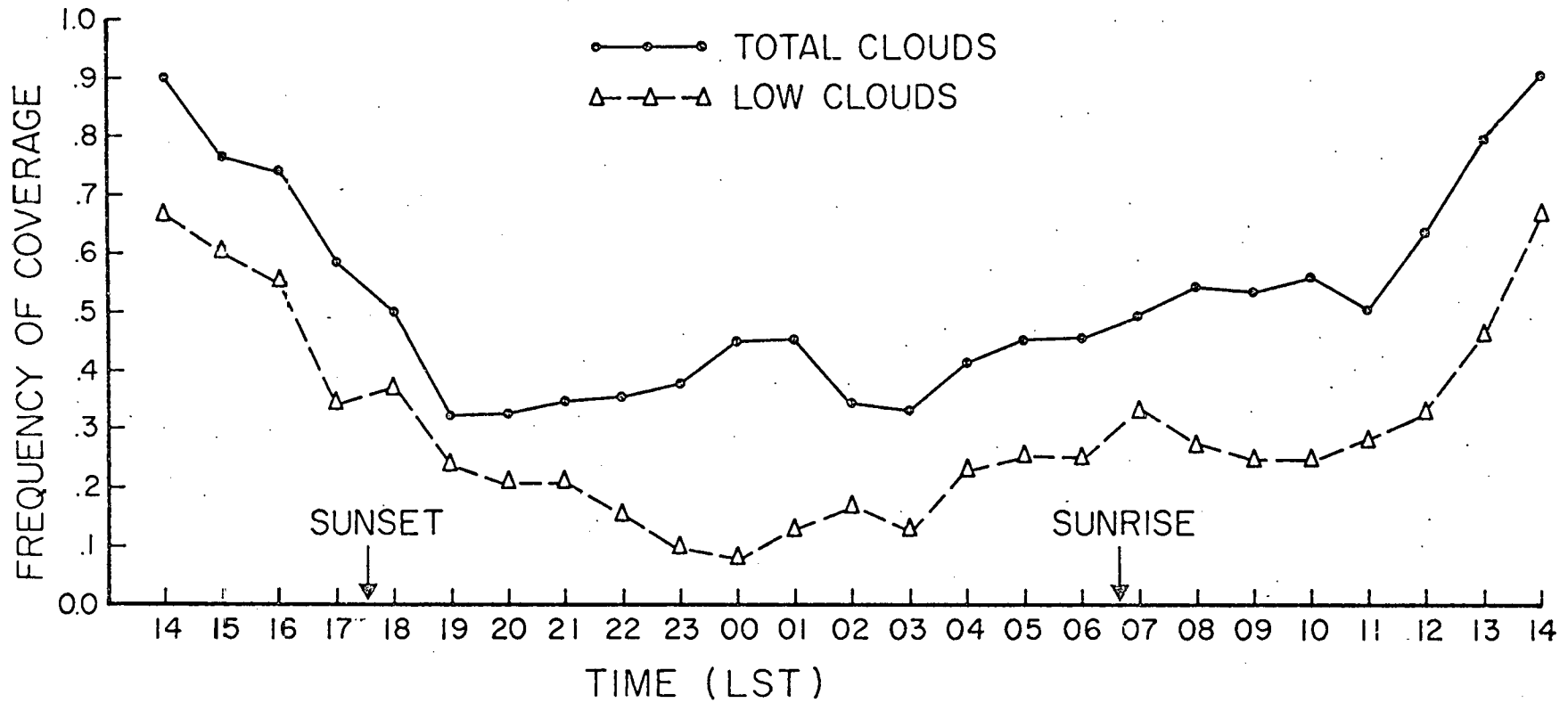


Fig. 4.1.3 The frequency that broken cloud coverage (> 5 tenths) existed during the Wangara Experiment is shown for both all cloudiness conditions and for only low clouds.

From Figs. 4.1.2 and 4.1.3 local weather characteristics can be deduced. Hay has some degree of cloudiness almost every afternoon with the bulk of these clouds having low bases. The clouds break up in the early evening although scattered conditions are reported during most nights. Low cloud activity begins again an hour or two after sunrise with broken skies prevailing by noon. The small amount of precipitation during the period, in spite of the frequent cloudiness, is a possible indicator of dry conditions in the lower troposphere. (Analyses of two-kilometers height revealed relative humidities generally below 30%.)

B. Surface Characteristics

The following parameters are examined for their mean diurnal profiles: surface temperature, nocturnal surface inversion, wind speed and water vapor mixing ratio.

The characteristics of the daily surface temperature trend and the existence of the surface inversion are illustrated in Fig. 4.1.4. Surface temperatures were obtained at a screen height of 1.2 meters. Traits include a maximum temperature at approximately two hours after local noon and a minimum shortly before sunrise. Rapid cooling is seen directly after sunset with slow nocturnal cooling following this period. Rapid warming occurs during the morning hours. This profile is typical of what one would expect for Hay, Australia in the winter (Trewartha, 1968).

Surface inversions were determined from three-hourly radiosonde data with 50-meter height resolution. Criteria to determine the existence of a surface inversion were:

1. An inversion base was sought up to 300 m above the surface.

SURFACE TEMPERATURE AND INVERSION CHARACTERISTICS

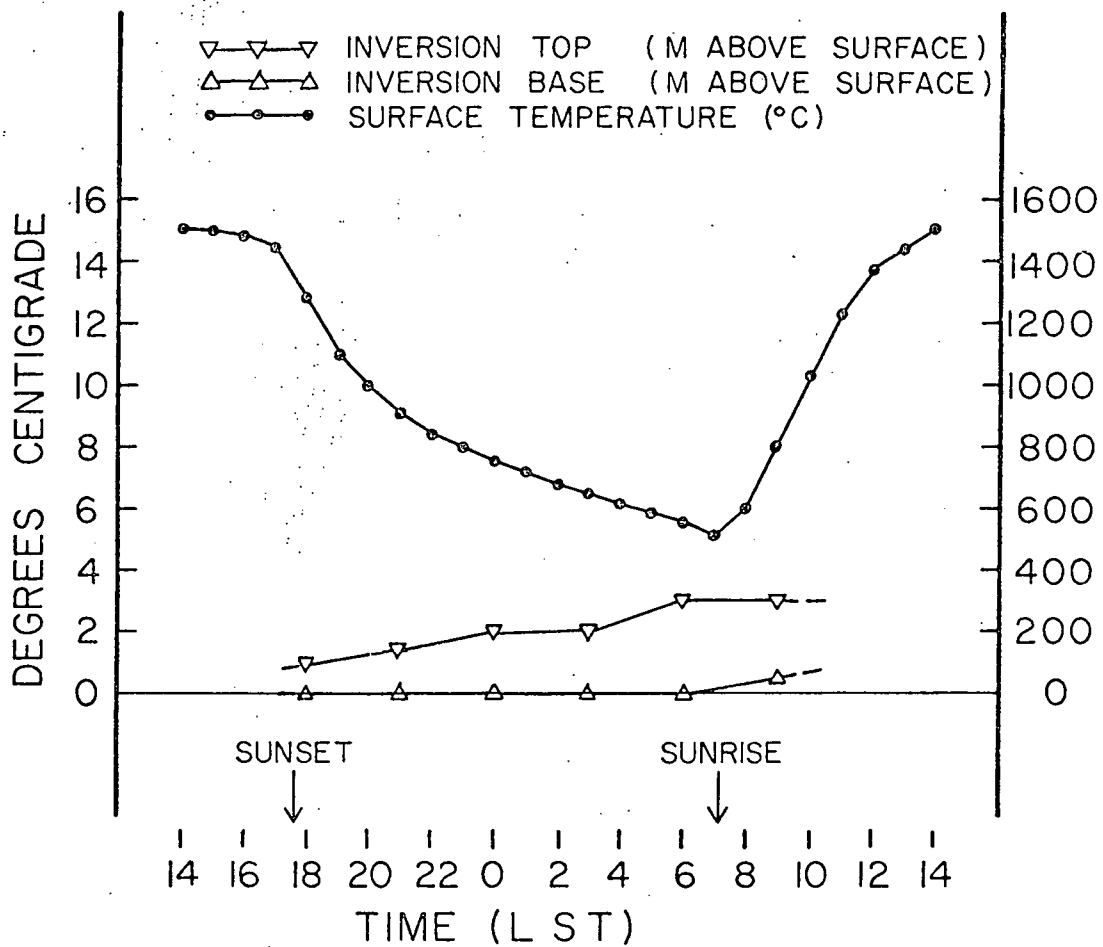


Fig. 4.1.4 Compositied surface temperature and inversion characteristics for the Wangara Experiment.

2. An inversion occurred if at any level, the next level above had a temperature greater than or equal to that of the particular level.
3. The inversion top was determined for a particular height where, in the next two consecutive levels (100 m), there existed two consecutive drops in temperature.

In spite of the three-hour resolution which prevented a more precise determination of when and how the inversion was actually created and destroyed, the basic character of the inversion can be deduced. The inversion forms near sunset and builds to a depth of 100 m within a half hour after this time. The thickness continues to grow during the night up to 300 m height while the base remains on, or very close to, the ground. Near sunrise the inversion base begins to dissipate and rises 50 m within an hour after sunrise; it is completely destroyed in an hour or two after this time.

Of particular importance is the daily consistency of the surface inversion throughout the Wangara Experiment. Of the thirty-nine days with temperature profile data, only during one day did the inversion not occur at all (this was in conjunction with a very strong wind occurrence). The inversion formed by 1800 local standard time (LST) and lasted through 0900 LST for all but seven days. It started as early as 1500 LST one day and lasted as late as 1200 LST twice. Finally, the base formed and stayed consistently at the surface (measured from one meter above the ground) and its top did not vary by more than 50 m from its average profile for most of the cases. With such persistence, it would be interesting in future research efforts to associate the diurnal

occurrence of the surface inversion with that of the other surface parameters mentioned in this chapter.

Average surface wind speeds and water vapor mixing ratios are given in Fig. 4.1.5. Surface wind was determined as an average of four measurements between 2 and 16 meters, inclusive. These heights were used to obtain a good representation of the near-surface wind effect with a minimum of variance from surface friction. The average wind speed for the entire period is a breezy 4.3 m/sec. Diurnal dependence is evident from the graph. At night, wind speeds are on the average slightly greater than 3.5 m/sec. This picks up quickly at sunrise to 5.5 m/sec. The wind then calms down approximately two hours before sunset to its nocturnal values.

The water vapor profile also shows a diurnal variation, although it is not as pronounced as for the wind speeds. It is interesting to observe the steady rise in surface water content after sunrise while the area is still probably under the nocturnal inversion influence. This can be an indication of morning evaporation from the surface and is further investigated in the next section (Sasamori, 1970). Once the inversion breaks (around 1000 LST) and the lower atmosphere is mixed through a deeper layer, the absolute humidity levels off and then declines for the rest of the day. An average water vapor mixing ratio for the entire period is a relatively low 5.36 gm/kg. Relative humidities at the surface (calculated from average surface temperatures) range from a low of 50% in the afternoon, 60% in the early evening, and a high of 87% just before sunrise.

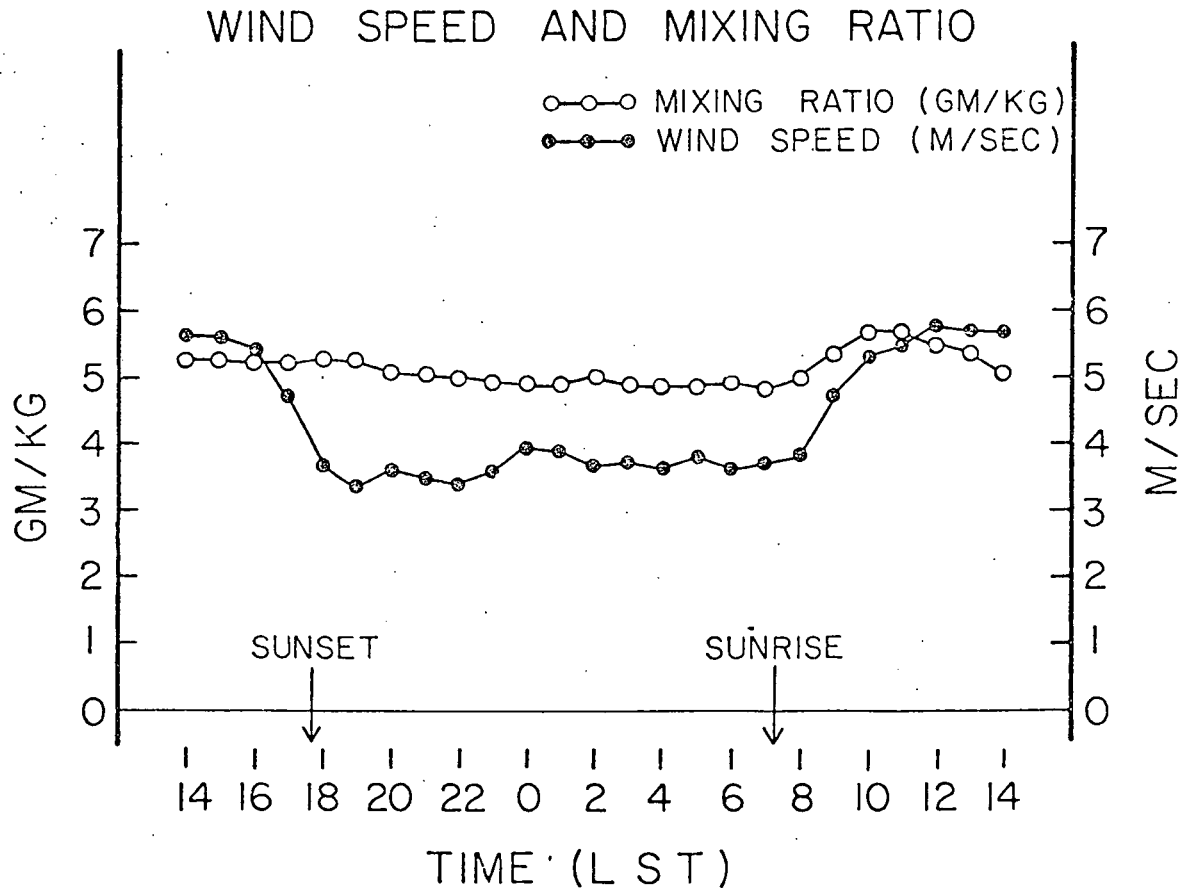


Fig. 4.1.5 Compositied surface wind speed and mixing ratio for the Wangara Experiment.

4.2 Surface Energy Parameters

A. Diurnal Characteristics

The diurnal profiles of the four components that make up the surface energy budget are presented in Figs. 4.2.1a, b. Positive flux is measured towards the ground for the radiation term and away from the ground for the other three terms. The figures illustrate how sensible, latent and ground heat flux jointly remove energy from the surface during the day in order to balance the incoming radiation and behave in the opposite direction at night. This result compares favorably to studies by Philip (1957), Elliot (1964), Sasomari (1970) and Sellers (1974).

Of the four energy fluxes, the ground heat flux and the net radiation profiles were taken directly from the measured data. Although the net radiation is considerably larger in magnitude than the ground heat flux, both fluxes appear to behave in a like manner. Ground heat flux is approximately one half as large as net radiation at night and one fourth as large during the day. Both fluxes have their greatest negative values shortly after sunset. During the daylight hours there seems to be a proportional rise and fall in magnitude with that of the solar altitude. Greatest values occur near local noon.

In Fig. 4.2.1b, both sensible heat flux and latent heat flux were calculated indirectly from the data. Sensible heat flux was calculated from hourly near-surface temperature and wind gradients. The equations used in this calculation come from Businger et al. (1971) and the procedure is demonstrated in the Appendix. These equations were used in a similar form for the Wangara Experiment by Melgarejo and Deardorff

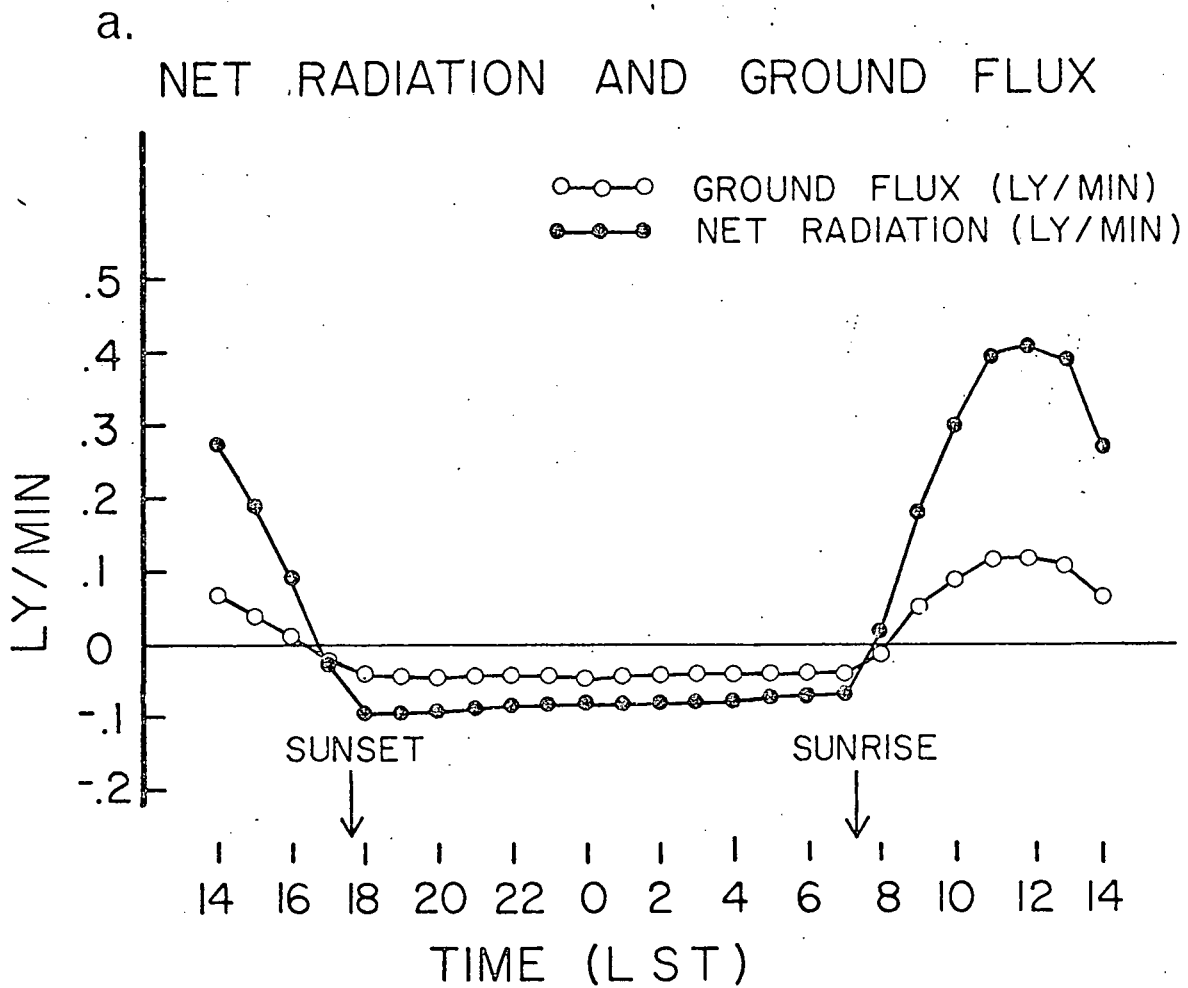


Fig. 4.2.1a,b The composited cycles of the four parameters in the surface energy equation are presented. The hourly mean latent heat flux was calculated as a residue of the other parameters.

b.
SENSIBLE HEAT AND LATENT HEAT FLUX

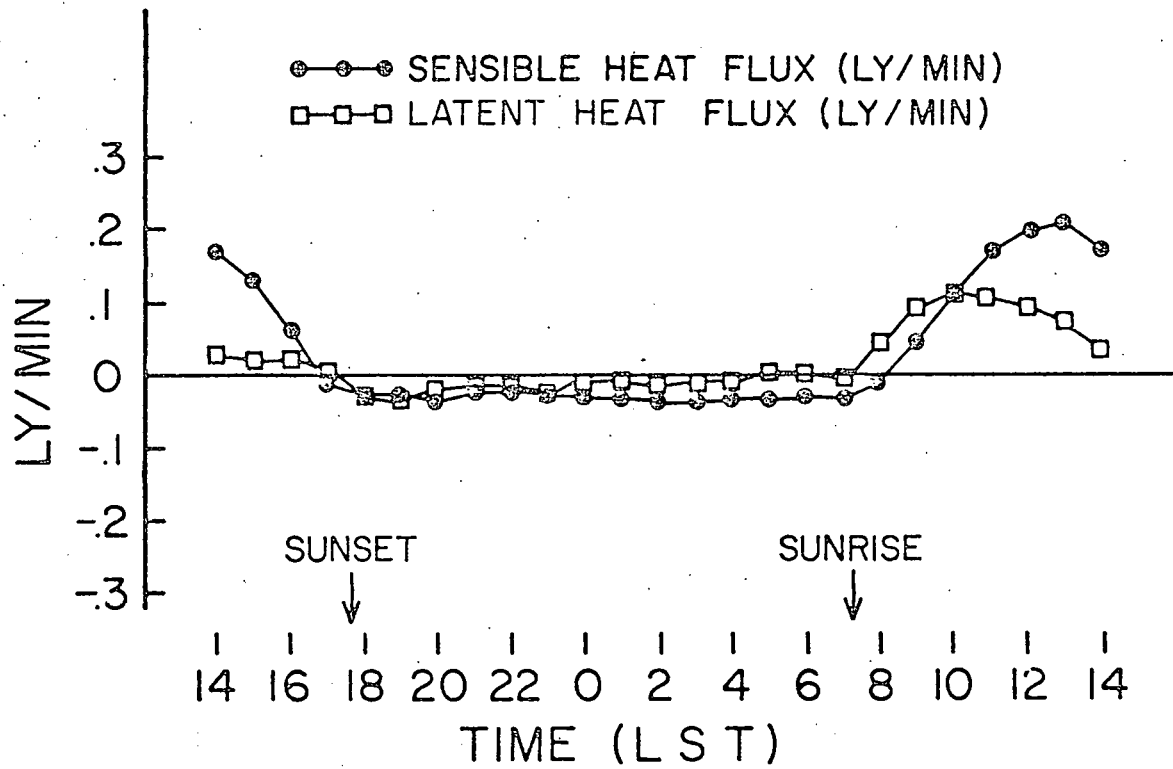


Fig. 4.2.1 (Continued)

(1974) and Yamada and Mellor (1975). A comparison with their research showed daytime values in fairly good agreement, but Melgarejo and Deardorff's nighttime calculations were approximately 1/2 to 2/3 as large in magnitude (which they also state they were to Clark's unpublished measurements). If it is assumed (as suggested by Clark, 1970) that in a dry stable environment nocturnal latent heat flux can be equal to zero, then a larger negative value of heat flux, as found here, is required to balance the measured values of net radiation and ground heat flux. (This assumes that there is not a substantial storage or advective term.)

In this research, latent heat flux was calculated as a residue of the hourly averages of the three other components in the surface energy budget. As expected, the values are very small, or zero, during the night. The positive values in the morning hours are supported by the increase in surface moisture shown in Fig. 4.1.4. Except for the period shortly after sunrise, values of latent heat flux remain significantly smaller in magnitude than those of sensible heat flux, a consequence of the dry soil conditions. Sasamori (1970) has demonstrated that once the excess soil moisture is evaporated, an increase in sensible heat flux with an accompanying decline in latent heat flux is usually observed.

B. Fluctuations in the Energy Parameters

Net radiation, ground flux, sensible heat flux and surface temperature were examined for relative deviations from their normal diurnal trend under eight different weather categories.² Since latent heat flux

² These categories were chosen because of their similarity to those used by air pollution modelers to predict low level stability (Hosler, 1961; Turner, 1964 and Slade, 1968).

was calculated as a residue of the other three energy parameters, it was not studied here. The results are shown in Figs. 4.2.2a-d.

In all cases a positive deviation means the measured value is more positive in direction. Temperatures are warmer and cooler for positive and negative deviations, respectively. Also, for the three energy parameters, an enhancement in absolute flux would require a negative deviation during the night and a positive deviation during the day.

Best interpretations of these graphs are made by looking at contrasting categories (i.e., 1 and 2, 3 and 4, 5 and 8 and 6 and 7). Since the fluxes are all less at night than during the day, relative deviations are generally larger for the night data. Also, peaks near sunrise and sunset are caused by sign changes in the diurnal trend. A brief summary of the results is presented below.

Surface temperature behaves in accordance with our normal experience (Trewartha, 1968). Although little variation is noted for afternoon temperatures, there is less cooling at night under cloudy and windy conditions and more cooling during calm, clear nights. Greatest deviations occur just before sunrise. The continuous negative deviation in Category 8 could also be the result of a dry air mass behind a cold front.

As expected, net radiation shows a definite cloud dependence while wind speed appears to have little or no effect on radiation. This cloud effect will be investigated further in the next chapter.

As in its diurnal cycle, relative deviation in ground flux behaves very similarly to that of the net radiation; although, wind conditions seem to have a slight effect. The wind effect (Category 3) might actually be related to the surface temperature deviation. Since ground

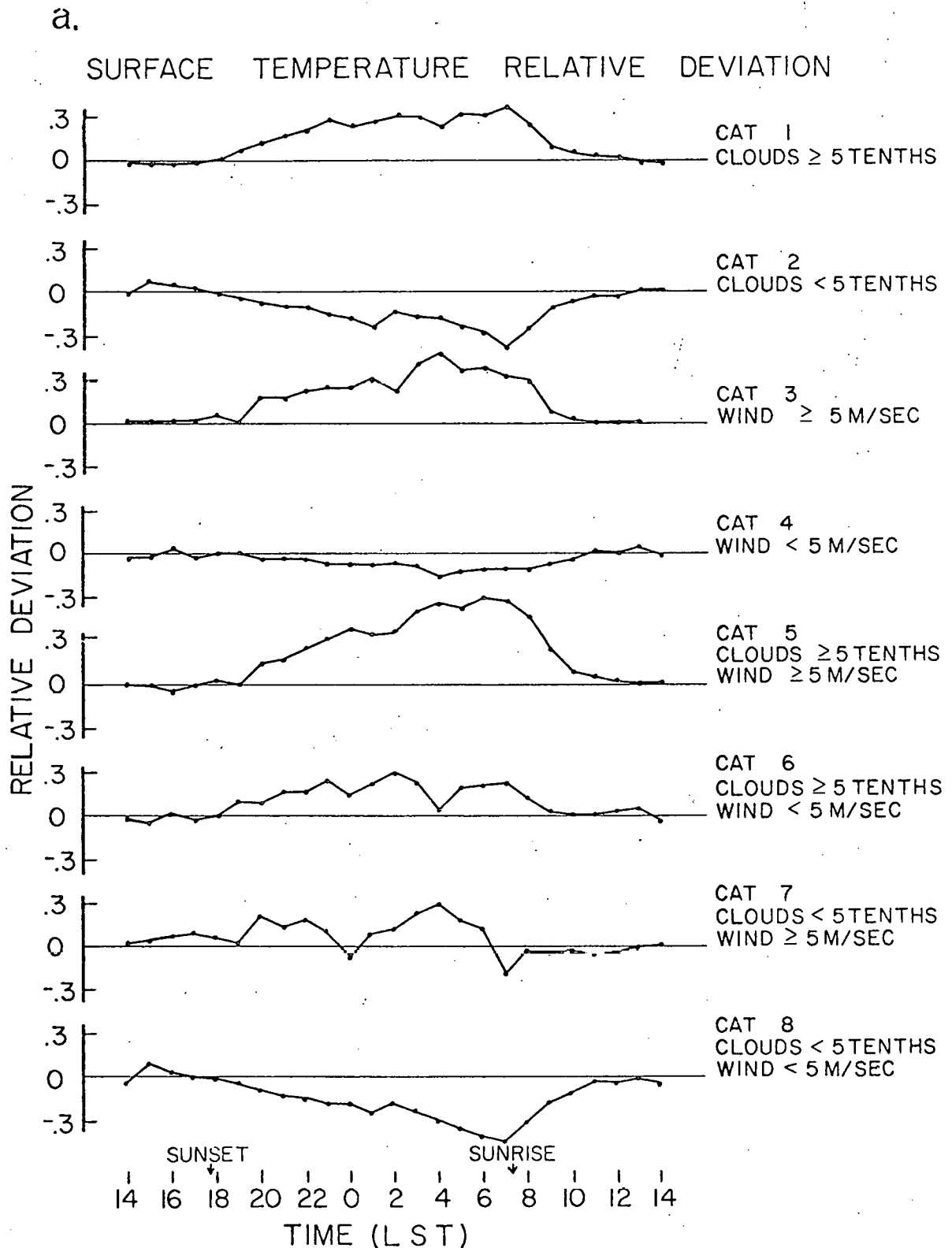


Fig. 4.2.2a-d Relative deviations from their mean diurnal composite under eight cloud and wind categories are shown for surface temperature (a), net radiation (b), ground flux (c), and sensible heat flux (d).

b.

NET RADIATION RELATIVE DEVIATION

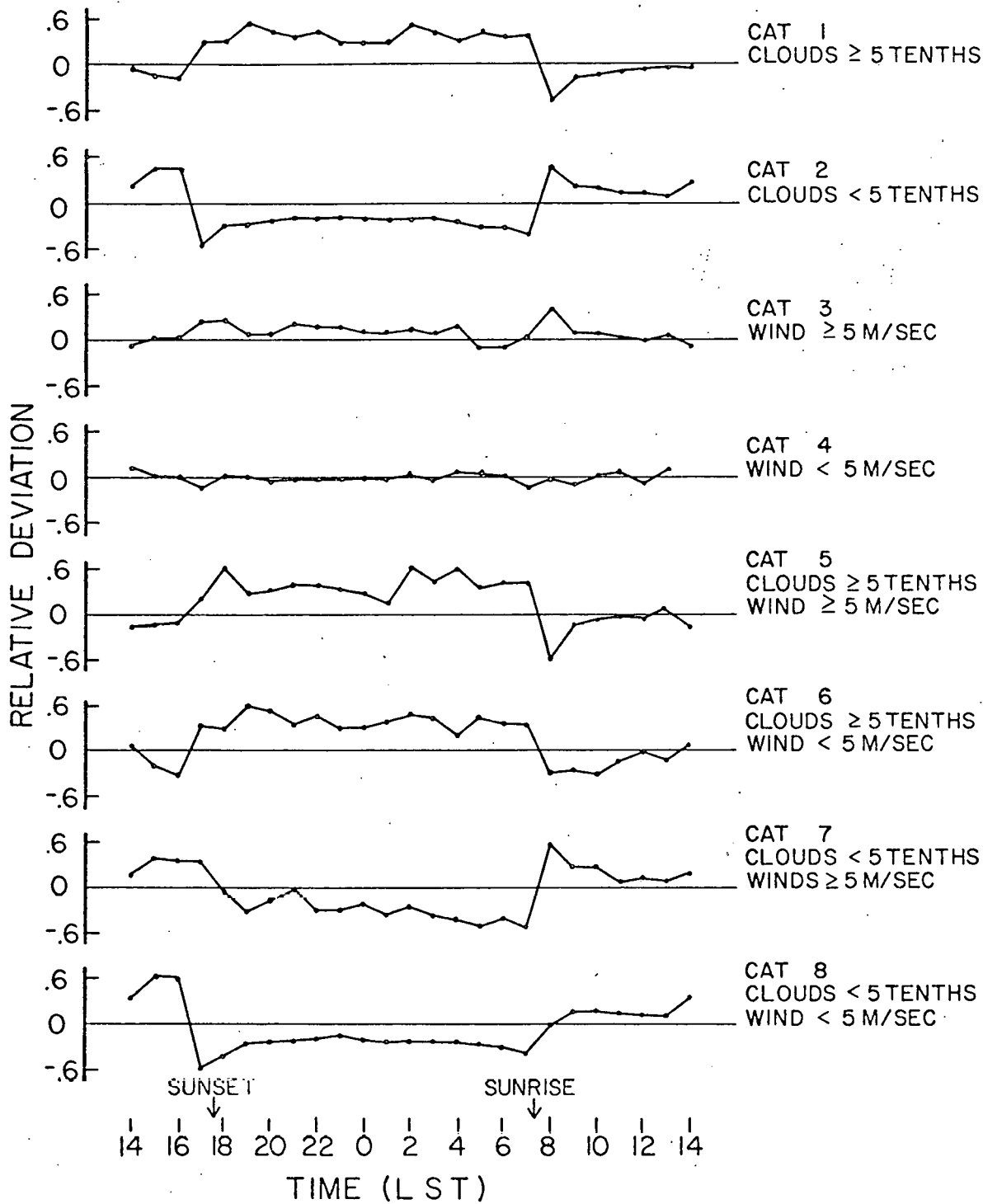


Fig. 4.2.2 (Continued)

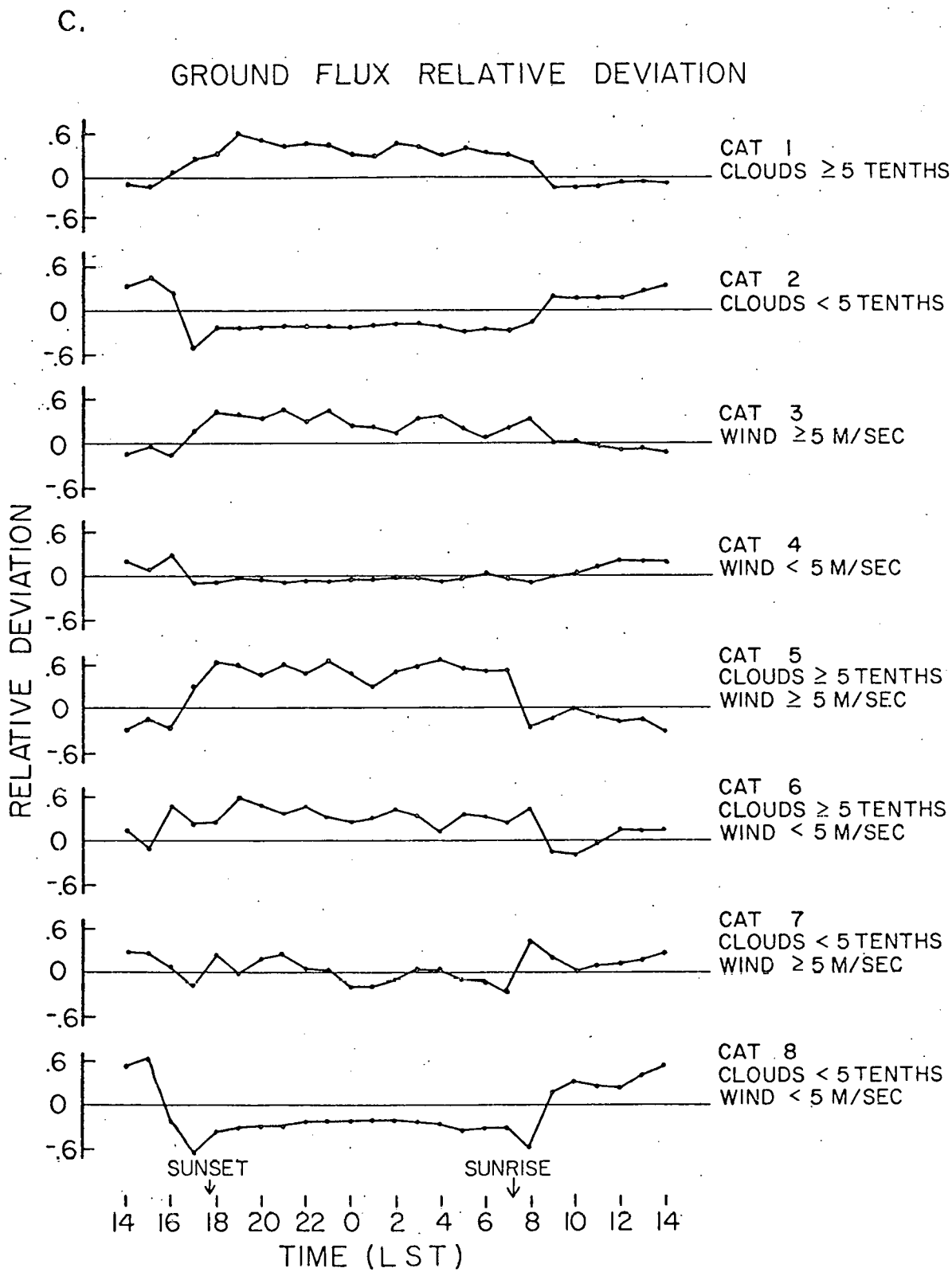


Fig. 4.2.2 (Continued)

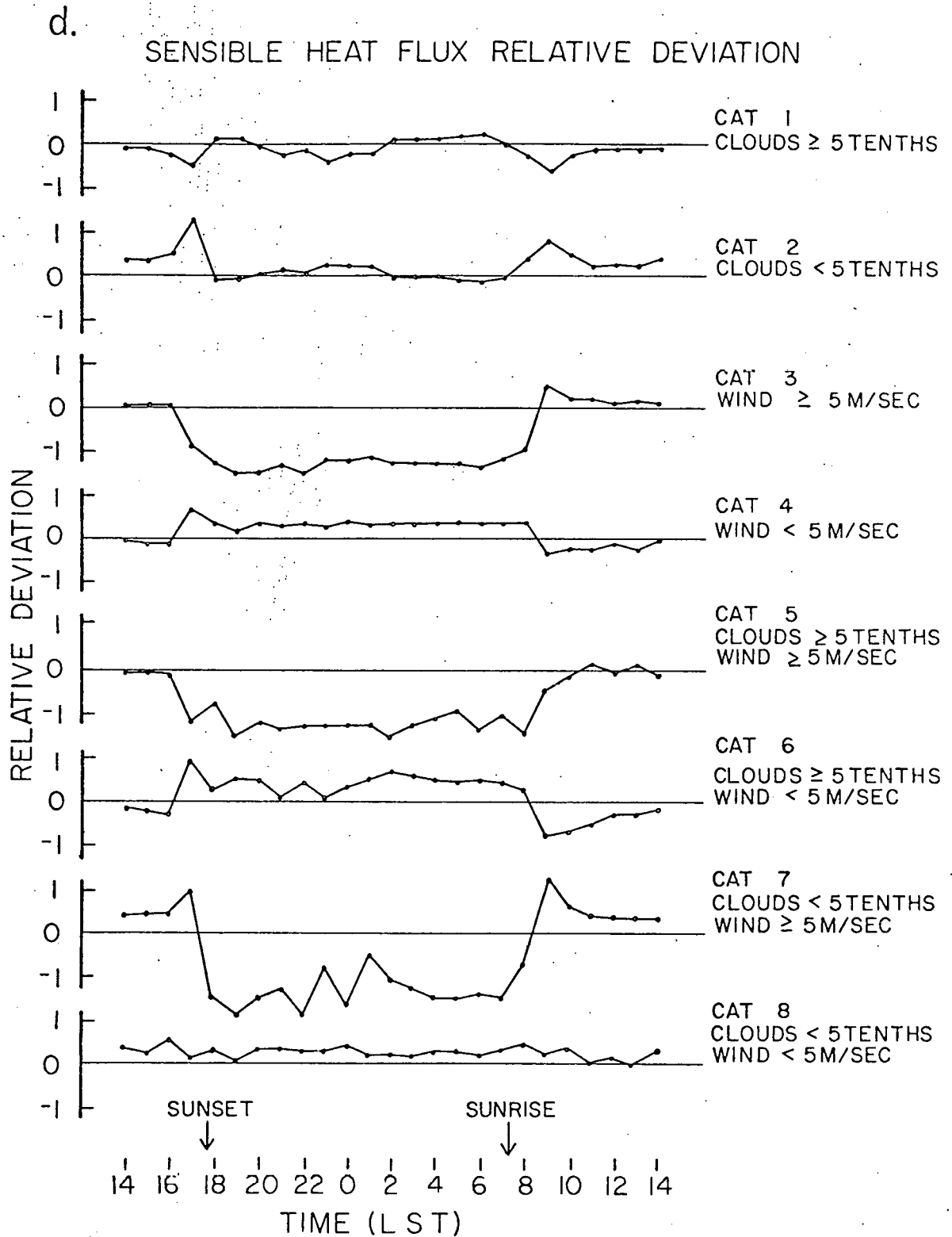


Fig. 4.2.2 (Continued)

flux is sensitive to the temperature gradient just below the surface, a nocturnal warming trend as in Category 3, Fig. 4.2.2a, could also cause less resultant ground flux towards the surface (Philip, 1957). Largest deviations are in Categories 5 and 8. These could be related to either net radiation or surface temperature.

Since the sensible heat flux equation is directly proportional to the surface wind speed (see Appendix), it is not unexpected to note that the wind categories dominate the heat flux deviations. In spite of large nocturnal warming trends in Categories 3 and 5, the large negative deviations in heat flux show that the lower temperature gradient did not reverse. (This is further supported by the persistence of the surface inversion mentioned previously.) Cloud changes - and the resulting influence on the temperature lapse rate - did have an effect on afternoon heat flux values in Categories 1 and 2. Largest deviations in sensible heat flux are in Categories 6 and 7 where both wind speed and the change in temperature gradient could be affected the most.

4.3 Chapter Summary

In this chapter, mean meteorological properties of the Wangara data were examined and the significance of the diurnal cycle was emphasized. Specific diurnal characteristics of the four components of the surface energy budget, net surface radiation, sensible, latent and ground heat flux were also illustrated. Evidence shows that broad-scale cloud or wind changes could possibly influence the diurnal trend of these parameters in a predictable manner. Good correlations occurred between cloudiness and net radiation and windiness and sensible heat flux. A possible relationship between surface temperature and ground heat flux

was also indicated. Finally, a strong relationship between net radiation and ground heat flux was noted.

The fact that the radiative flux is considerably larger in magnitude than the other fluxes supports the importance of the radiation term in the energy budget; hence, deviations in the normal trend could affect, as shown above, the other terms as well. These deviations will be more closely studied in the next chapter.

5. RESULTS: ANALYSIS OF NET RADIATION FOR THE WANGARA EXPERIMENT

Chapter 3 described theoretical aspects of net radiative flux and suggested methods to indirectly calculate this flux from surface-obtained meteorological parameters. It is the intent of this chapter to determine how accurately the Wangara data can be parameterized by these methods.

5.1 General Cloud Effects on Net Radiation

Chapter 4 presented the mean diurnal trend of the net surface radiation and demonstrated relative deviations from this profile due to cloudiness and winds. Figure 5.1 further illustrates net radiation changes under three sky conditions: periods of cloud free skies¹, periods that report skies at least half cloudy and periods with less than half the sky cloudy. From this figure it is noted that cloud influence increases more rapidly as cloud cover increases. This is discussed further in a later section.

5.2 IR Radiation

Net radiation was examined between the nighttime hours, 1800 and 0700 LST, inclusive. This enabled IR radiation to be studied independently.

A. Net IR Radiation Under Clear Skies.²

The Brunt Equation discussed previously:

$$F_0 = \epsilon\sigma T^4(a - b\sqrt{e}) \quad 3.1.2$$

¹ A criterion of cloud cover less than 0.5 tenths was used in order to obtain a sufficiently large data sample. It is shown in a following section that this small cloud cover has very little effect on IR radiation.

² See previous footnote.

DIURNAL CHANGE IN NET RADIATION

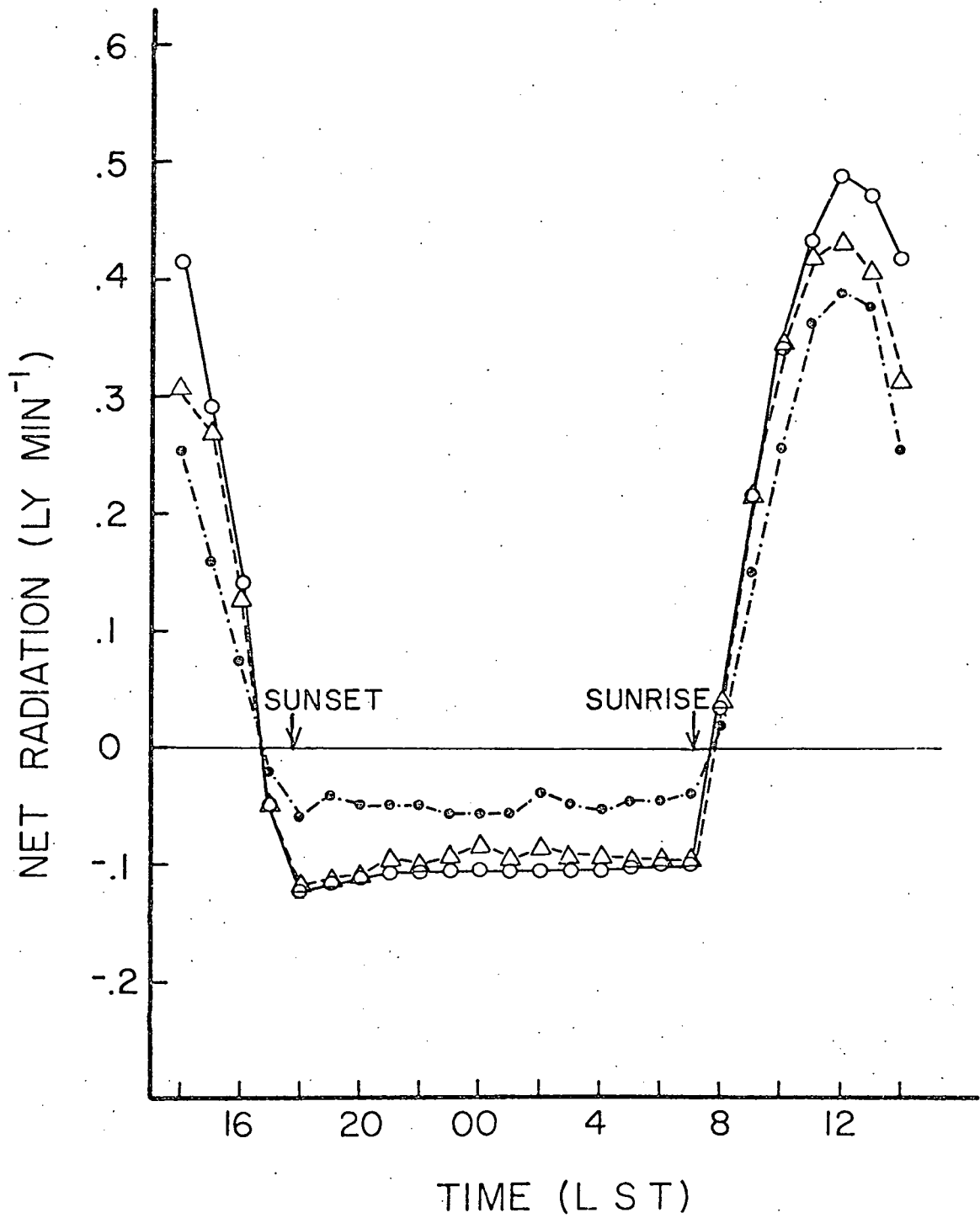


Fig. 5.1 Influence of clouds upon Wangara radiation data. Open circles are for clear skies, triangles for skies < 5 tenths cloudy, and closed circles for skies \geq 5 tenths cloudy.

requires only dry and wet bulb temperatures from the Wangara data in order to evaluate net IR radiation under clear skies. A method of least squares was used to determine the constants from a data sample of 122 measurements during the night:

$$a = .351 \pm .025$$

$$b = .050 \pm .010$$

These values coincide very well with the post-1950 results shown in Table 3.1.2. The relatively small standard deviations can account for errors of $.02 \text{ ly min}^{-1}$ (19%) in net IR radiation. The fit to the Wangara data using mean temperature and moisture measurements is shown in Fig. 5.2.1.

Although there is no easy way to judge the accuracy of the daytime predictions, the night results appear acceptable. The IR correction suggested in Chapter 3.1B to account for substantially non-neutral conditions, especially for strong daytime unstable conditions during the day, might have improved the results; but without proper feedback concerning the accuracy of this approach, it was deemed impractical for this research.

For general application, it is possible that values of the constants a and b are subject to seasonal changes in temperature, moisture, dust and especially surface conditions (Brunt, 1952). These effects may need to be investigated on a site-specific basis, although the similarity of the Wangara results to those of the more moist European climates, suggest that they do not vary greatly.

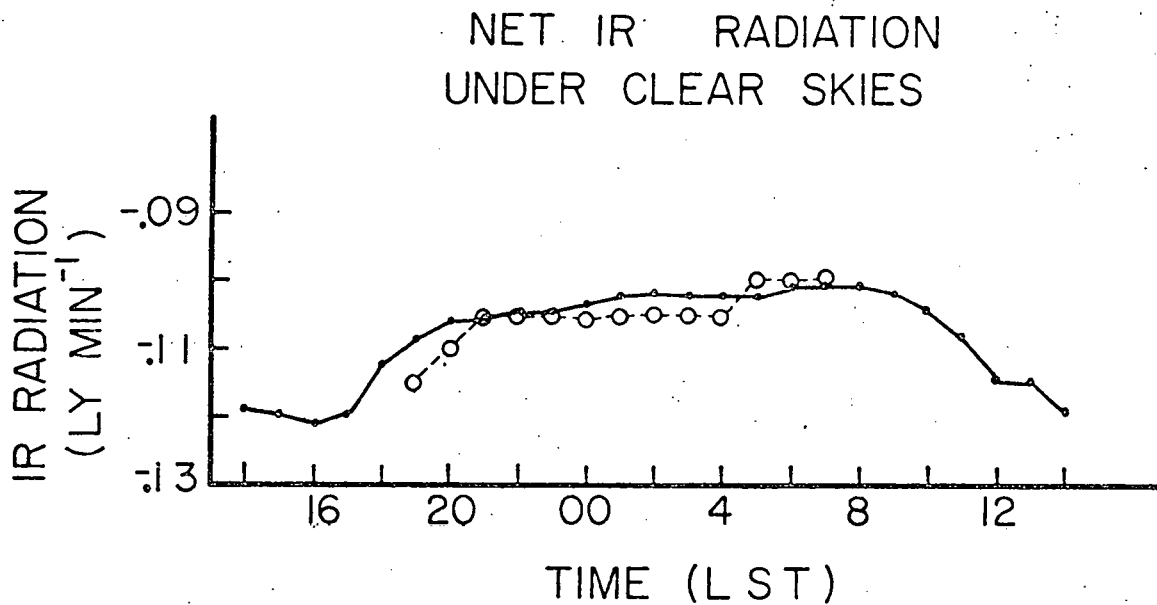


Fig. 5.2.1 Solutions to the Brunt Equation for the Wangara Experiment. The solid curve illustrates the predicted profile of net IR radiation under clear skies; the dashed curve represents mean Wangara measurements.

B. Cloud Effects on IR Radiation

Equation 3.1.3:

$$F_{o,n} = F_o(1 - Kn^m) \quad 3.1.3$$

and the calculated values of net IR radiation under clear skies were used to study the cloud effect on IR radiation. The following questions are examined in this section:

- (1) How accurately does Eq. 3.1.3 represent the Wangara data, and is IR attenuation by clouds a linear or quadratic effect ($m = 1$ or $m = 2$)?
- (2) What are the coefficients, K , (K -values) for the different cloud types and how do they compare to previously obtained measurements?
- (3) Do K -values have a nocturnal variation?
- (4) Under layered cloud conditions, is it more accurate to distinguish each cloud type (Eq. 3.1.4) or to evaluate the total sky cover as a whole?

Fourteen hours of nighttime data were analyzed both separately by hour and for an average of the entire night. The data were divided, as previously described, into three categories: Total Clouds, Only Low Clouds and No Low Clouds. The number of samples available for any particular hour and cloud type have been presented in Fig. 4.1.1. A computer-derived least squares fit was made for both $m = 1$ and $m = 2$ to determine the K -values for the data. In this computation, radiation measurements were given more weight when cloud cover was less than two-tenths or greater than eight-tenths. This was done to alleviate

unrealistic results caused by scatter in the mid-cloudiness region.³ Solutions for average nighttime K-values are presented in Table 5.2.1.

Table 5.2.1 Average Nighttime K-Values for Wangara Data.

Cloud Category	m	K-Value
Total Clouds	m = 2	.80 ± .04
	m = 1	.77 ± .04
Only Low Clouds	m = 2	.89 ± .05
	m = 1	.85 ± .05
No Low Clouds	m = 2	.64 ± .05
	m = 1	.63 ± .05

One notes that the standard deviations of the K-values are almost identical for both values of m. (This is also the case for the individual hours.) In both cases the solutions predicted effective radiation to within a 15% accuracy under five-tenths cloudiness and to only a 45% accuracy under total low cloud coverage. However, when radiation measurements were plotted on a graph versus cloud cover, it was found that qualitatively the quadratic solutions fitted the data better than the linear results. A subjective analysis showed that the linear solutions consistently overestimated the attenuation of net IR radiation under scattered cloud conditions: this favored a higher order solution. These results are illustrated in Figs. 5.2.2a-d for four selected times during the night (linear solutions are not shown).

³ Data points in the mid-cloudiness region were more scattered and tended towards less net IR radiation than the general trend. A possible cause of this characteristic is the chance of an isolated incident of clouds directly over the Funk radiometer at Station 5. As the skies become more cloudy, the scatter reduces as the likelihood of clouds overhead for all the stations increases.

CLOUD AMOUNT VS. IR RADIATION

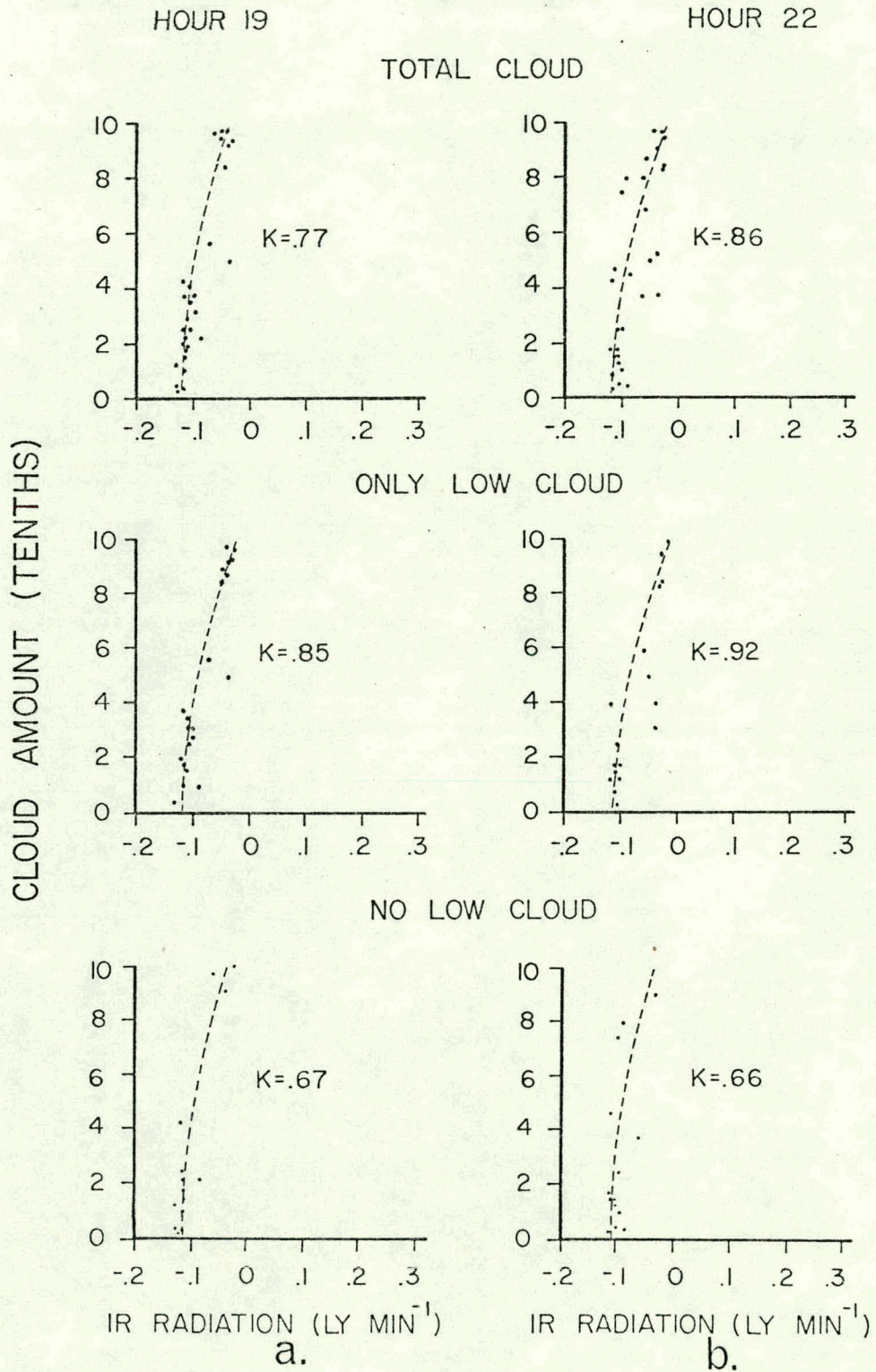


Fig. 5.2.2a-d Solutions to Eq. 3.1.3. Curves are for $m = 2$ and a K as indicated in each graph. The dots represent measured data.

CLOUD AMOUNT VS. IR RADIATION

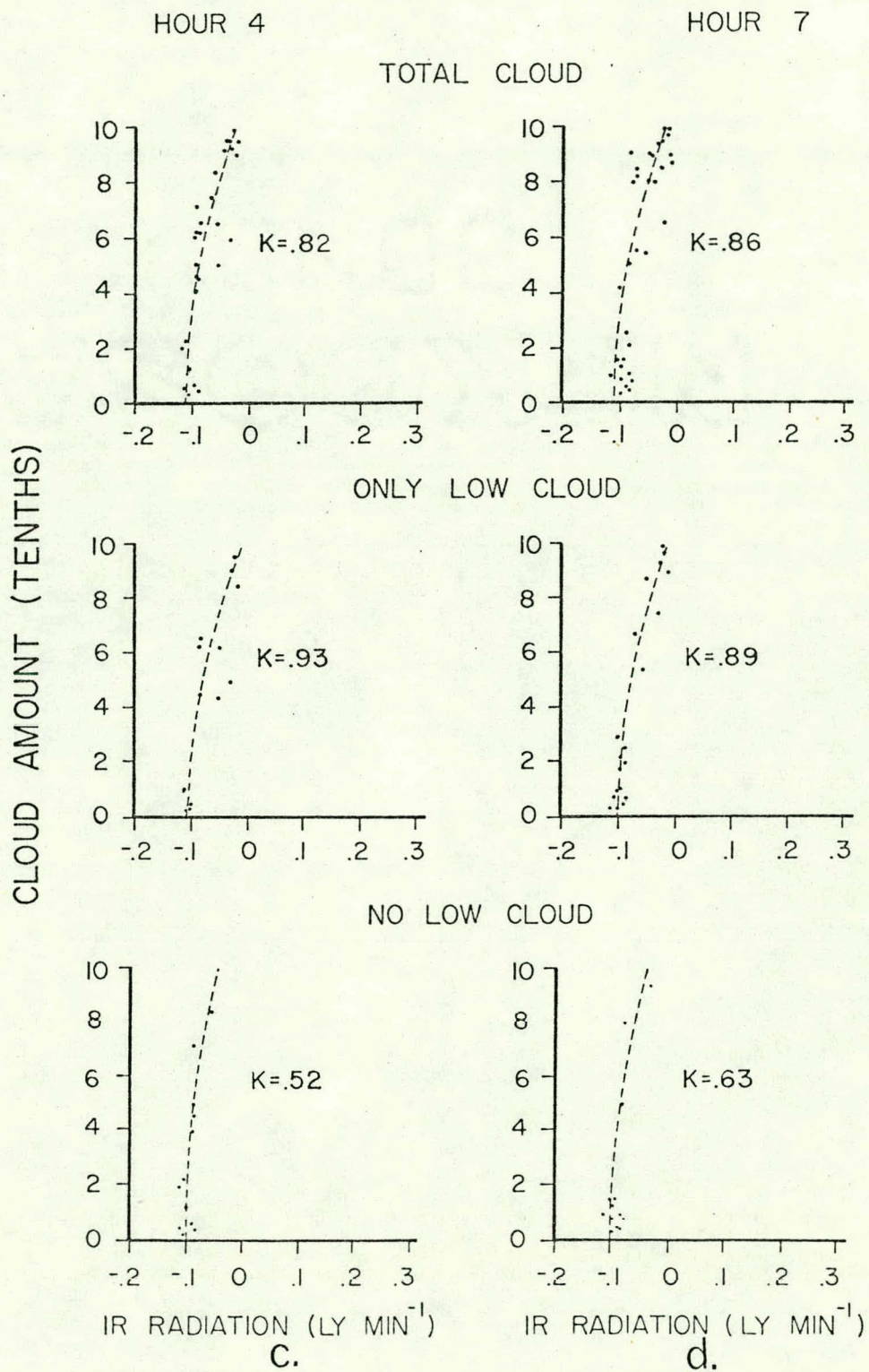


Fig. 5.2.2 (Continued)

Four time periods are presented in the above figures to demonstrate the similarities in the results for each cloud category. The remaining night calculations were similar to these solutions. Although K-values were obtained for each hour, deviations between each hourly value were within the accuracy of the least squares fit for any particular hourly calculation; hence, only the average K-values for $m = 2$ found in Table 5.2.1 will be used in this report.

As previously mentioned, a No Low Clouds category is used because the Wangara data did not quantify middle and high clouds separately. However, the K-value obtained for the No Low Clouds category in Table 5.2.1 appears close to values one would expect for middle clouds (see Table 3.1.3). In order to make a distinction between middle and high clouds, the entire fourteen-hour nighttime period was scanned for hourly reports that recorded either only middle clouds or only high clouds. Because of the limited data sample, a curve to represent the data was fitted subjectively. Figures 5.2.3a and b show the findings. The nonlinear effect ($m = 2$) is again demonstrated. K-values obtained are:

Middle Clouds $K = .64 \pm .06$

High Clouds $K = .51 \pm .09$

The K-values can now be compared to the previously obtained values in Table 3.1.3. The K-value for Only Low Clouds, .89, is within the range given for K_{10} in the table. From the range in values presented in the table, it can be assumed that the thickness and type of cloud probably is an important factor when determining cloud attenuation. In the Wangara data, low cloud overcast was often associated with the thicker Cu and Cb type clouds. This would require a higher attenuation coefficient than for a less massive St or Sc type cloud. For more precision

b.

HIGH CLOUDS VS. IR RADIATION

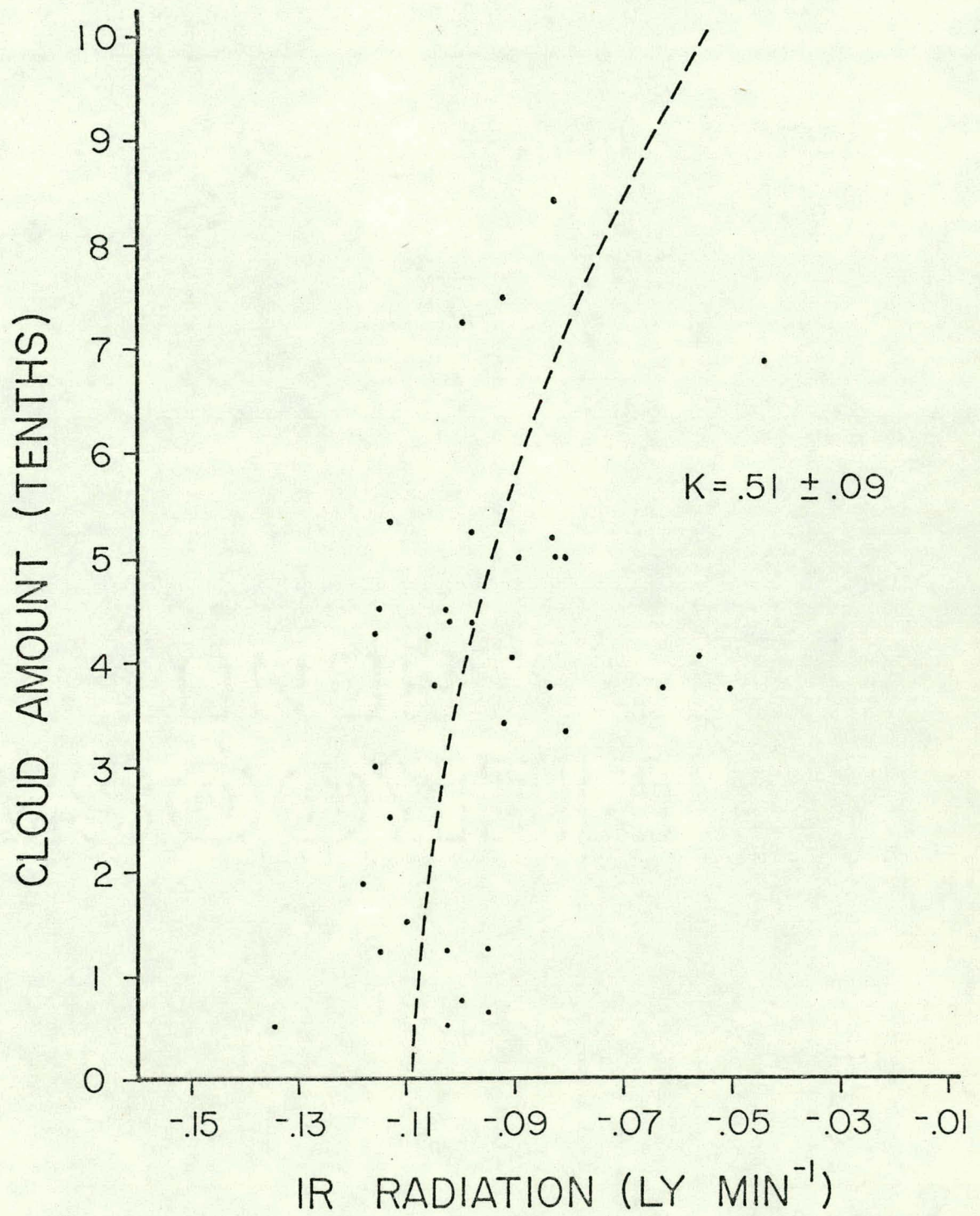


Fig. 5.2.3 (Continued)

in determining K-values, more measurements of particular type clouds under overcast skies need to be recorded.

As suggested previously, the K-value obtained for the No Low Clouds category actually is an indication of IR attenuation by middle clouds. In fact, this value is in the range of some of the higher middle cloud (K_{mi}) figures given in Table 3.1.3. As was suggested for low clouds, the particular characteristics of the middle cloud (type, thickness, and base) might be an important consideration when studying the effect on effective radiation.

The computation for high clouds in this report is higher than the values from Kondratyev's review (in Table 3.1.3). Because of the sparsity of high cloud ceilings greater than six-tenths (see Fig. 5.2.3b), it is probable that the K-value was overestimated. Although a curve was drawn that best reflected the data, it is possible that an extreme K-value could be estimated as low as 0.25 (average for Kondratyev's figures) from these data.

Finally, the K-value for the Total Clouds category, 0.80, appears to be a mean between the values for middle and high clouds, 0.64, and low clouds, 0.89. (Figure 4.1.3 showed that at night, low clouds occurred 60% of the time that broken cloud conditions occurred.) This determination of a mean K-value is similar to long-term radiation studies that use mean attenuation coefficients over an area (e.g.; Kondratyev, 1965; Berlyand, 1970 and Kumor, 1978). However, a method to determine a mean K-value is suggested here which would require only knowledge of the individual cloud type K-values and the approximate frequency of occurrence of each type of cloud. This procedure can

readily be put to use in a region where radiation measurements have not been made, but knowledge of individual cloud frequency exists.

C. Accuracy of the IR Parameterization

The final investigation in this section is concerned with the ability of the combined Brunt and cloud attenuation equation to predict the Wangara radiation data. The quadratic solution ($m = 2$) was used and K-values were treated both separately (K_{10} and $K_{no\ 10}$) and as a composite value (K_{Tot}). In the first case, middle and high clouds were again treated as a single category. Standard deviations of effective radiation are presented in Table 5.2.2. K-values or a combination of K-values in the table heading indicate the form of the equation used for the three cloud cover situations listed.

Table 5.2.2 Accuracy Standard Deviation of the IR Radiation Equations ($ly\ min^{-1}$).

Cloud Type Present	K-Values	
	$K_{Tot} = .80$	$K_{no\ 10} = .64$ $K_{10} = .89$
Low Clouds	.018	.018
Middle and High Clouds	.018	.016
All Clouds	.018	.020

For a nightly mean net IR radiation of .082 (all conditions), the above parameterization is accurate to within 20-24%. However as net IR radiation gets smaller under more cloudy skies, the relative accuracy decreases. Considering the scatter in the data and the relatively small magnitude of net IR radiation measured under cloudy skies, this error is

acceptable. Qualitatively, the curves in Figs. 5.2.2 and 5.2.3 fit the data very well.

Because of the scatter in the data, little can be concluded concerning the advantage of using an average K-value or a combination of K-values under layered cloud conditions. Slightly more accuracy is achieved with $K_{no\ 10}$ over K_{Tot} when only middle and high clouds are present; but when several cloud types are present, a composite value of K (K_{Tot}) produced better results than an additive effect from the individual cloud categories. There can be several reasons for this: one possibility is that the uncertainty in the K-value for both cloud categories created an cumulative error in the result. It is also possible that a combination of clouds present must be treated as a single entity and therefore can not be separated into individual effects. In order to resolve this problem, more research needs to be done to study the effect of clouds in combination with each other.

D. Summary

This section has shown that IR radiation can be parameterized hourly through relatively simple equations requiring only knowledge of surface temperature and moisture and cloud conditions. Although cloud attenuation coefficients were determined for low, middle and high clouds, there appears to be enough diversity in cloud characteristics to require more investigations on the effects of specific type clouds. Overall, the use of a mean K-value for a particular area will give a reasonable estimate of net IR radiation. This reinforces previous investigations concerned with radiation studies over longer periods of time. For either long or short periods, the quadratic effect of cloud

attenuation is an important consideration when estimating the radiation budget.

5.3 Residual Radiation

The IR parameterization discussed in Section 5.2 was subtracted from the daytime net radiation measurements in order to obtain a residual radiation. This calculated residual radiation is assumed to contain mostly SW radiation plus an additional error term from the IR parameterization during the daytime. Furthermore, this residual radiation is examined with net SW radiation equations because of the inability to estimate surface albedo from the data.

A. Residual Radiation Under Clear Skies

Before one can describe the turbidity during the Wangara experiment, it is first necessary to determine SW radiation at the top and the bottom of the atmosphere. The top three curves shown in Fig. 5.3.1 were evaluated from Eq. 3.2.2 for SW influx through a horizontal surface at the top of the atmosphere. The curves reflect the increase of solar influx during the month of the experiment.

With a constant surface albedo, α , of 0.15 assumed, $Q_{g,n}$ (solar radiation absorbed by the ground) could be converted into Q_{go} (solar radiation reaching the ground) and Eq. 3.2.3 could then be used to approximate turbidity from the residual data. A preliminary analysis using this equation resulted in the optical air mass, M , overcorrecting for low solar altitude (the turbidity coefficient decreased with solar angle). If the turbidity coefficient is assumed to be diurnally constant, a modification of M needs to be made. Houghton (1974) and Robinson (1962) have suggested such a modification for M :

DAYTIME RADIATION AT HAY, AUSTRALIA

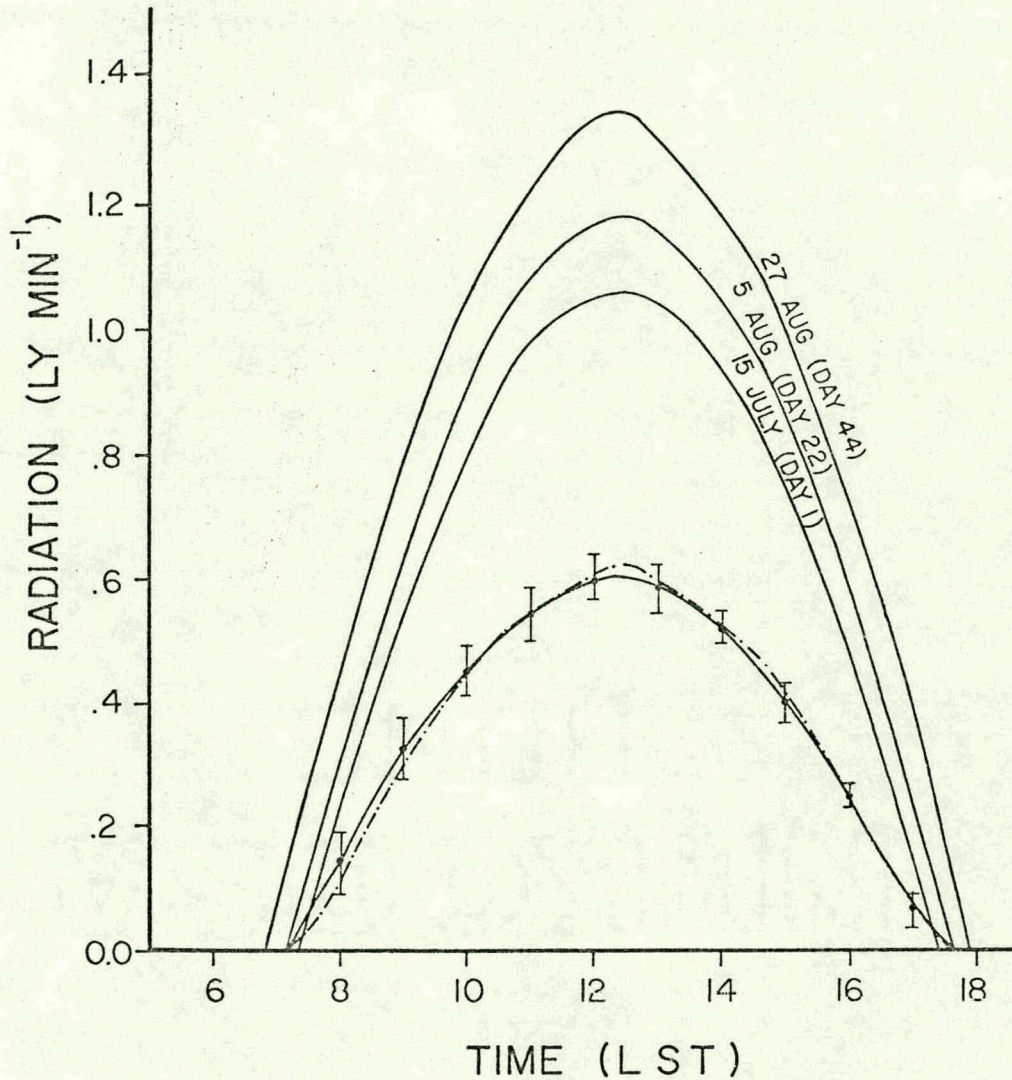


Fig. 5.3.1 The change in SW influx at the top of the atmosphere is shown in the top three curves. The lower solid curve represents the composited cycle of residual radiation at the surface for the Wangara data with the error brackets as indicated for each hourly average, the dash-dotted curve is the solution of Eq. 5.3.1 for Day 22.

$$Q_{g,n} = (1 - \alpha) Q_s 10^{-x(M^{1/s})} \quad 5.3.1$$

where x is a combination of τ_r , τ_z and B in Eq. 3.2.3, and $1/s$ is an empirical constant. Robinson found a value of 1.25 for s .

A least squares evaluation of Eq. 5.3.1 for a data sample of 62 radiation measurements under clear skies⁴ between the hours of 0800 and 1700 LST, inclusive gives:

$$x = 0.16 \pm .03$$

$$s = 2.0 \pm .8$$

The findings of this evaluation are illustrated in the bottom two curves of Fig. 5.3.1. The dash-dotted curve represents the predicted values for Day 22 while the solid curve shows the diurnal trend of the actual data with error brackets to indicate the standard deviation for each hour. These deviations are largely due to the monthly increase in solar influx. Both curves are assumed to go to zero at sunrise and sunset for Day 22.

Although the standard deviation of the coefficients could account for up to a 35% error in the radiation estimate under low sun angles, the ability of Eq. 5.3.1 to predict the Wangara measurements on an hourly basis is clearly seen in the graph. It would be interesting to test Eq. 5.3.1 with direct SW radiation measurements. If the solutions were similar, seasonal values of x need only be obtained to approximate the diurnal SW absorption by the ground.

⁴ A criterion of cloud cover less than 1.5 tenths was used in this section to obtain an adequate data sample. As a justification for this criterion, a comparison was made between surface temperature, moisture and net radiation for totally clear skies and skies with cloud cover less than 1.5 tenths which resulted in little or no change in values.

Assuming the residual radiation represents net SW radiation fairly close under clear skies, the magnitude of x , 0.16, indicates a medium turbid atmosphere for Hay, Australia as compared with values given by Flowers et al. (1969) in Chapter 3.2A. This value would decrease slightly if it is necessary to reevaluate the magnitude of the surface albedo upwards.

In this section, no attempt is made to compare turbidity variations with moisture and dust. It is assumed that generally with more clouds in the sky, there is more moisture in the atmosphere and the turbidity increases. This is parameterized in the next section as a cloud effect rather than a change in turbidity.

B. Cloud Effects on the Residual Radiation.

The primary goals of this section are:

(1) To determine the practicality of Eq. 3.2.4 to make a reasonable residual radiation prediction with clouds and to determine the degree of accuracy for using the equation:

$$Q_{g,n} = Q_{go}(1 - Cn^m) \quad 3.2.4$$

(2) To determine the coefficient, C , (C -values) for different cloud types and to see how they vary under a change in solar angle.

(3) To determine values of m that best describe the data.

Data were again separated into three cloud categories; times with approximately common solar angles were combined into five groups so that hours 12 and 13 were treated together, 11 and 14, 10 and 15, 9 and 16, and 8 and 17. The advantage of these combinations is that cloud distributions in the morning and afternoon could better complement each other.

C-values for each cloud category were obtained from estimates of residual radiation under clear and cloudy skies. Radiation values under clear skies were calculated from Eq. 5.3.1 as an average of the two hours that made up each group. Radiation values under cloudy skies were determined from graphical extrapolation of the data with cloud cover greater than eight-tenths. These results are displayed in Fig. 5.3.2 and Table 5.3.1. As a precaution for possible errors in the above analysis, a range of C-values was calculated from the data and are also presented in Table 5.3.1.

The large range in calculated C-values could account for errors greater than 50% in the prediction of residual radiation under cloudy skies. For less than cloudy skies, the accuracy of Eq. 3.2.4 is better (this will be demonstrated shortly). The small magnitude of the radiation and the individual characteristics of each cloud could be partial reason for these wide ranges in values. Furthermore, the sample size for overcast middle and high clouds was limited since the majority of afternoon overcast skies during the Wangara experiment consisted of low cumuliform clouds. More precise results could be obtained if only one cloud type is studied at a time rather than a cloud group; however, the relative location of the sun with respect to the individual clouds will probably limit the ability to predict solar attenuation by Eq. 3.2.4 on a short term basis.

In spite of these limitations, some general observations can be made. In all cloud categories attenuation changes little for the three highest solar angles; hence, an average C-value for each category is presented in Table 5.3.1. During these three periods, the observed attenuation for Total Clouds, 0.70, and Only Low Clouds, 0.74, compare

RESIDUAL RADIATION UNDER CLEAR AND CLOUDY SKIES

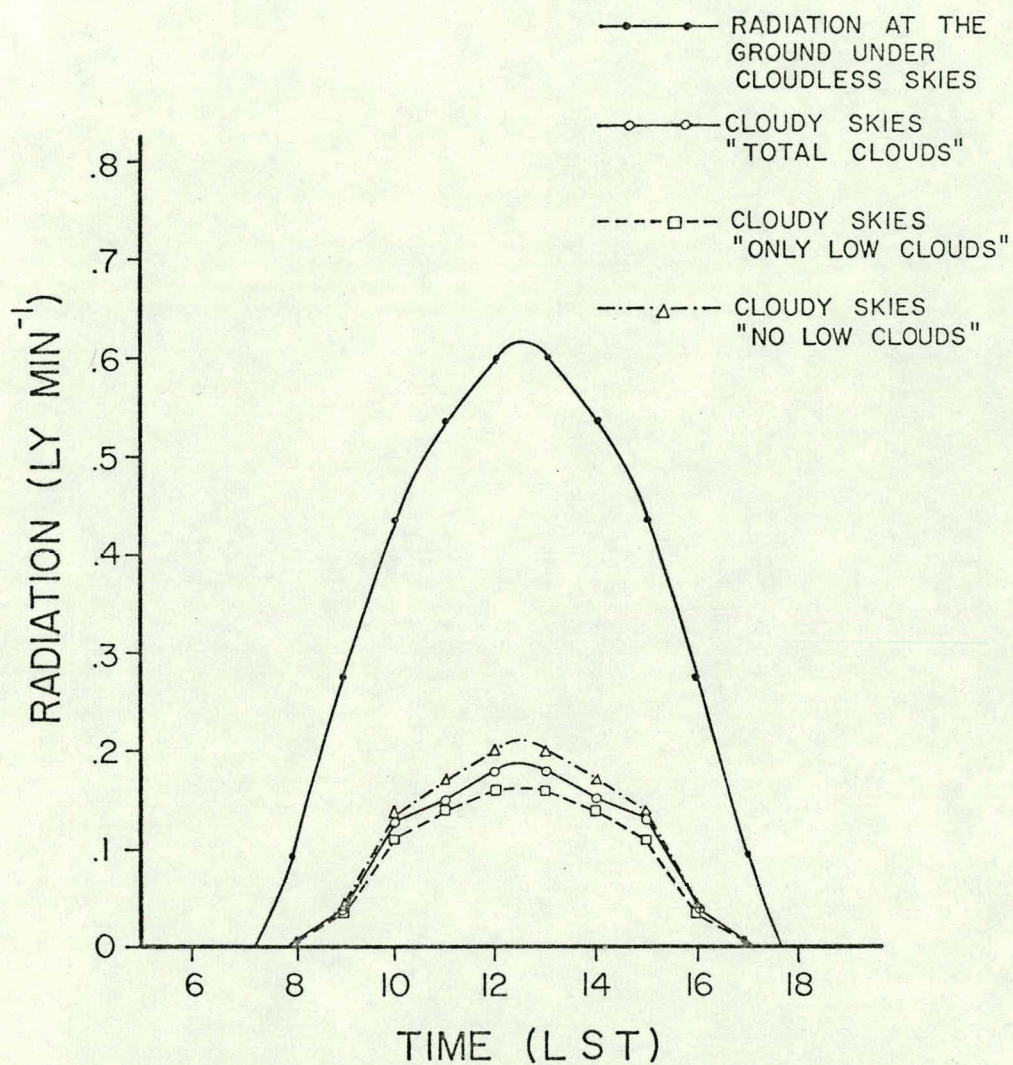


Fig. 5.3.2 A comparison between residual radiation measurements under clear skies and under cloudy skies for three cloud categories is presented.

Table 5.3.1 C-Values for Residual Radiation.

Time (LST)	Average Solar Altitude (Day 22)	Total Clouds C-Value	(Range)	Only Low Clouds C-Value	(Range)	No Low Clouds C-Value	(Range)
12&13	38°	.70	(.60-.80)	.73	(.65-.80)	.67	(.50-.70)
11&14	35°	.72	(.60-.80)	.74	(.65-.80)	.68	(.55-.75)
10&15	28°	.69	(.50-.85)	.74	(.60-.85)	.68	(.45-.75)
Average of the Above		.70		.74		.68	
9&16	19°	.85	(.55-.90)	.87	(.60-.90)	.85	(.55-.90)
8&17	7°	.95	(.60-1.0)	.95	(.60-1.0)	.95	(.50-1.0)

favorably to those given for low clouds in Table 3.2.2. However, the figures given for No Low Clouds (probably containing Ac and As) were higher than values for middle clouds previously suggested. Only the lowest estimate (0.50) compared to Kondratyev's values. For solar angles less than 20° , the attenuation increases, but considerable uncertainty in C-values does not allow this increase to be substantiated.

C. Accuracy of the Net Radiation Parameterization During the Daytime

In this section, solutions of the exponent, m , are chosen for the five time combinations and comparisons are made between the two methods of using C-values in this research. Since the previously derived parameterization of IR radiation is included in these calculations, these results reflect the ability for both IR and residual radiation (approximately equal to SW radiation) to be parameterized.

The exponential fit of Eq. 3.2.4 was calculated by using fixed radiation values from Fig. 5.3.2 for clear and cloudy skies. Standard deviations were calculated for values of m between 1 (linear) and 4 (fourth ordered). This calculation is dependent upon the accuracy of the other procedures used in this parameterization. Therefore, a value of m was chosen for each cloud category and time period because of its ability to substantially improve the fit of the next lowest value of m .

Figures 5.3.3a-e illustrate the results of this study. Solutions of m and C are shown in each graph. The data points represent a residual radiation as extrapolated from the net radiation measurements and a predicted value of IR radiation.

In spite of the uncertainties in computing C-values, these graphs qualitatively indicate a good parameterization of the data. The best results appear to exist for the Total Clouds and Only Low Clouds

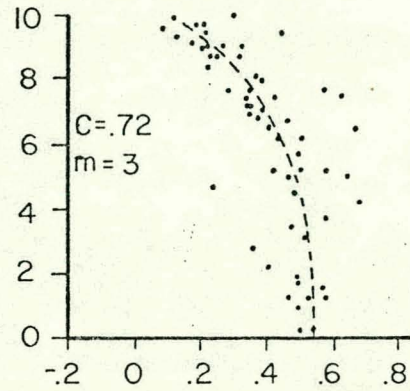
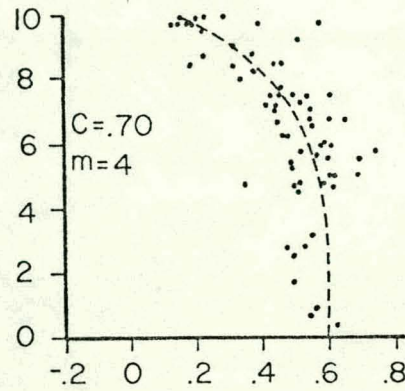
Fig. 5.3.3a-e Solutions to Eq. 3.2.4. Data points are determined from measured net radiation data and Eq. 3.1.3 for IR radiation.

CLOUD AMOUNT VS. RESIDUAL RADIATION

HOUR 12 & 13

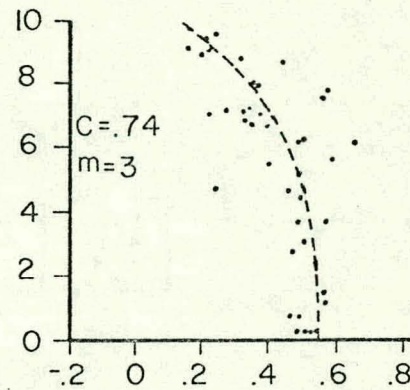
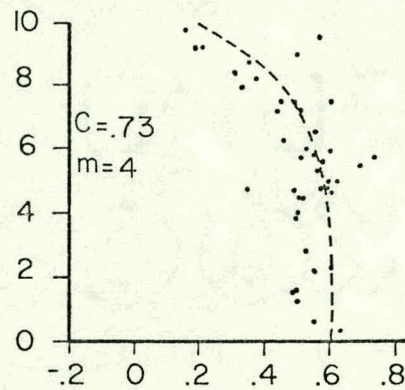
HOUR 11 & 14

TOTAL CLOUD

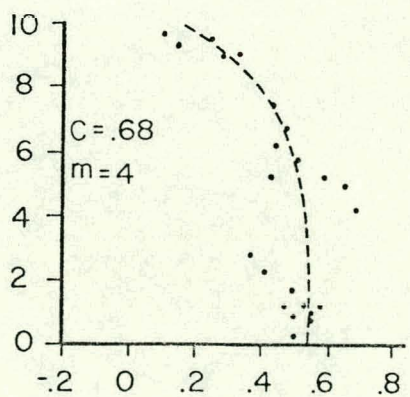
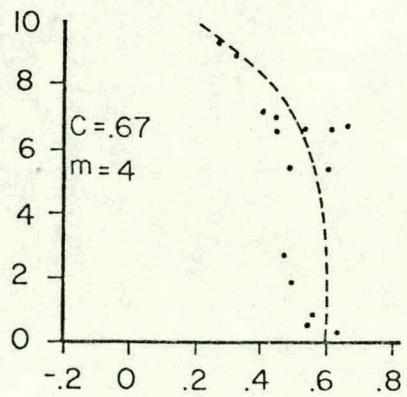


ONLY LOW CLOUD

CLOUD AMOUNT (TENTHS)



NO LOW CLOUD



RADIATION (LY/MIN)

RADIATION (LY/MIN)

a.

b.

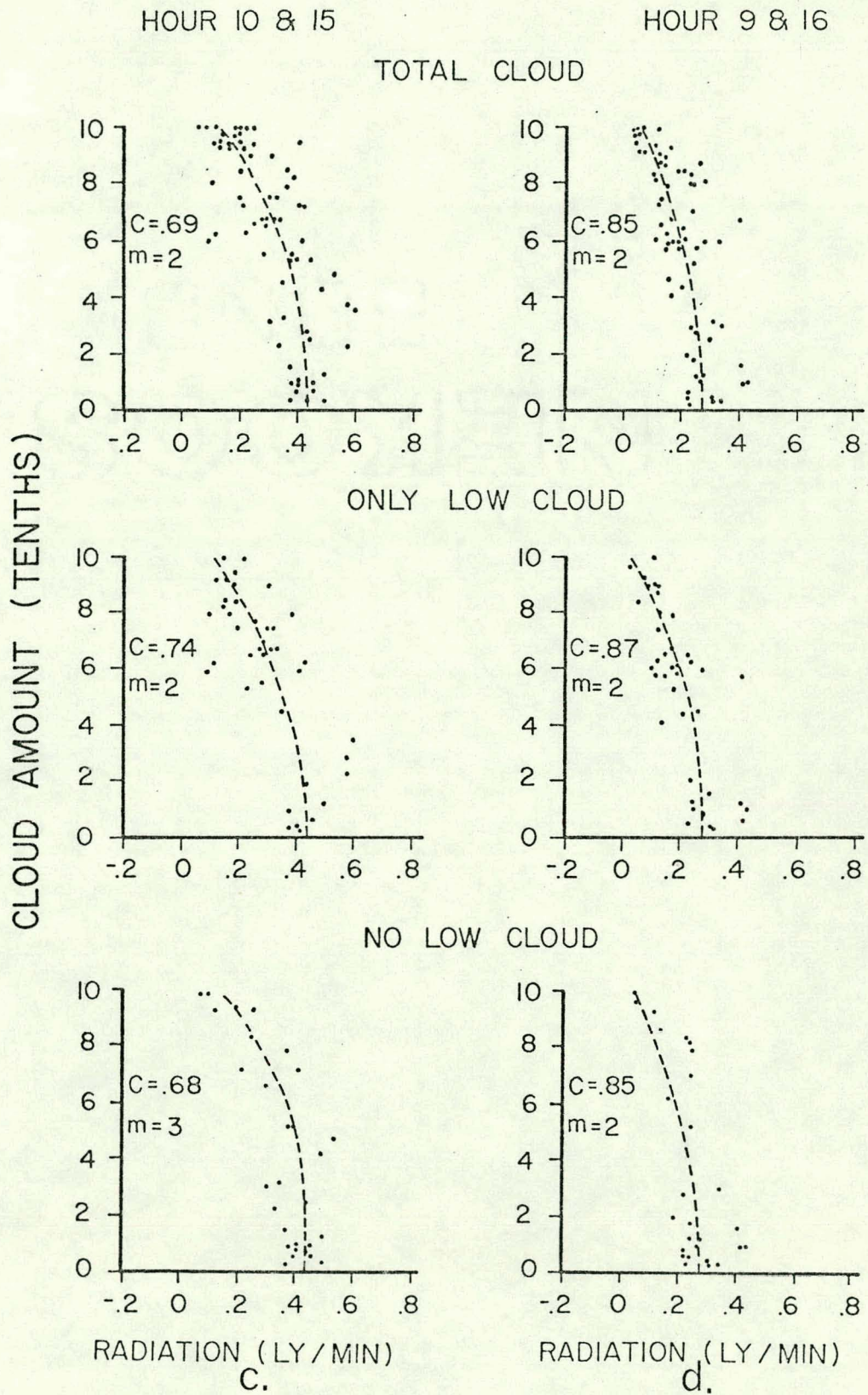
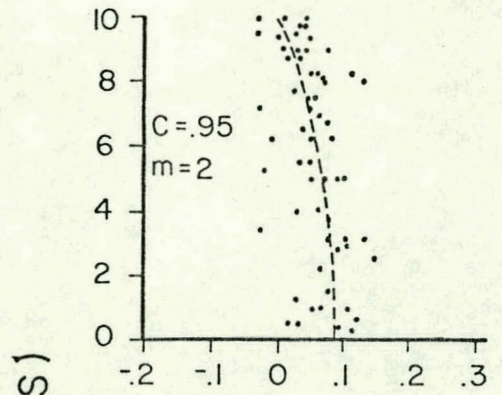
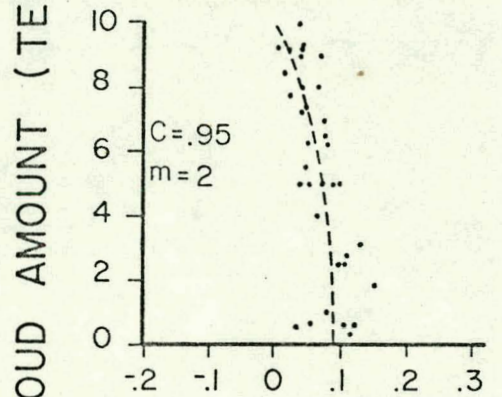


Fig. 5.3.3 (Continued)

HOUR 8 & 17
TOTAL CLOUD



ONLY LOW CLOUD



NO LOW CLOUD

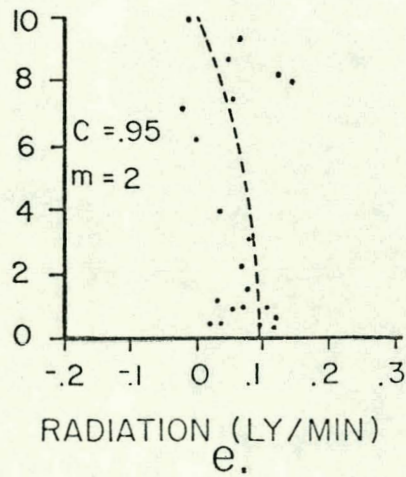


Fig. 5.3.3 (Continued)

categories at the higher solar angles. For the time period closest to sunrise and sunset the relative error is larger because the magnitude of incoming radiation is small. Also during this time, the shape of individual clouds probably becomes more important to solar attenuation as a result of an increase in SW scattering at lower solar angles.

Once again an excess scatter in the data is noticed in the mid-cloudiness region. It is possible that the cloud averaging technique used in this experiment could distort some of these measurements. Significant differences in readings could result depending upon whether or not direct sunlight is reaching the Funk radiometer at Station 5. However, as the distribution and cloud cover increased, this distortion should be reduced.

As previously stated, the rate at which clouds attenuate both IR and SW radiation (as judged by the residual radiation) is less under scattered conditions than for broken skies: attenuation increases rapidly as the sky becomes more overcast. This can especially be seen in Fig. 5.3.3 for high sun angles and for clouds with higher bases. When the sun is lower in the sky, attenuation increases more for less cloud cover. Nevertheless, a second order solution seems plausible for the times just before sunrise and sunset.

The accuracy of the above curves is summarized in Table 5.3.2. Standard deviations were calculated for low clouds, no low clouds and all clouds together. The selected values of m is placed in parentheses next to each calculation. Finally, a mean residual radiative flux, \bar{Q}_n , has been calculated for each time period in order for relative accuracies to be seen.

Table 5.3.2 Standard Deviation of Daytime Net Radiation Equations
(ly min^{-1}) and value of (m).

Time (LST)	C-Values	Cloud Type Present		
		Low Clouds	Middle and High clouds	All Clouds
12 & 13 $\bar{Q}_n = .496$	$C_{no\ lo} = .68$ and/or $C_{lo} = .74$ $C_{Tot} = .70$.098 (4) --	.074 (4) --	.118 (4) .094 (4)
11 & 14 $\bar{Q}_n = .427$	$C_{no\ lo} = .68$ and/or $C_{lo} = .74$ $C_{Tot} = .70$.085 (3) --	.077 (4) --	.098 (2) .089 (3)
10 & 15 $\bar{Q}_n = .332$	$C_{no\ lo} = .68$ and/or $C_{lo} = .74$ $C_{Tot} = .70$.092 (2) --	.066 (3) --	.087 (2) .091 (2)
9 & 16 $\bar{Q}_n = .225$	$C_{no\ lo} = .85$ and/or $C_{lo} = .87$ $C_{Tot} = .85$.070 (2) --	.067 (2) --	.068 (2) .070 (2)
8 & 17 $\bar{Q}_n = .047$	$C_{no\ lo} = .95$ and/or $C_{lo} = .95$ $C_{tot} = .95$.031 (2) --	.031 (2) --	.037 (2) .037 (2)

On the average, deviations of less than 20% are observed for the periods near noon. These amounts are of the same order of magnitude as for the IR parameterization. As before, the relative error increases as the mean radiation gets smaller either by more cloud attenuation or by lower sun angle. Standard deviations are approximately 30% for Hours 9 and 16 and rise sharply up to 80% for Hours 8 and 17. Although the No Low Clouds category does not show any larger error than the other two categories, a larger data sample, especially under near cloudy skies would probably give more confident results.

In the case where all clouds were examined together, the difference in accuracy between using a composite C-value or a combination of C-values is approximately the same. As in the discussion on cloud attenuation with IR radiation, the degree of scatter in the measurements and the possible cumulative error in the C-values causes a comparison to be unreliable. It is hypothesized that as in the IR study, a mean C-value for the month or season can be obtained from the climatological frequency of the cloud types for an area.

D. Summary

This section has shown that the Wangara data set can be used to parameterize net radiation to within 20-30% during most times of the day. A turbidity coefficient of 0.16 was determined with the assumption that the surface albedo remained diurnally constant (.015). Also, a factor of \sqrt{m} was found to best represent the extinction of the residual radiation under clear skies. Whereas an attenuation coefficient of 0.74 at high solar angles for low clouds was found to be comparable to other studies, the accuracy obtained for C-values at lower sun angle or for higher type clouds was limited. This degree of uncertainty can possibly

be reduced in future studies if direct SW radiation is measured with specific-type clouds. It is speculated that in these cases a larger data sample would probably reduce the C-values given in this study. The value of m might also be reduced slightly although the nonlinear effect of cloud attenuation appears quite evident.

This nonlinear effect could be of major significance to global surface energy modelers. If energy budgets are calculated under the assumption that cloud attenuation behaved in a more linear manner, an overestimation of SW radiation would occur under scattered cloud conditions. Finally, with more accurate values of m and C determined for different climatological regions, diurnal radiation budgets can then be calculated for large areas of the globe without the need for direct measurements.

6. CONCLUSION

This paper has used the hourly Wangara boundary layer data to substantiate previously derived empirical equations of the surface radiation budget. These equations only require measurements taken by a surface observer in order to be evaluated. A parameterization was made for IR radiation. Daytime residuals were then determined from this parameterization subtracted from measured net radiation data. This residual radiation was assumed to represent net SW radiation to a high degree. Residual was assumed to represent net SW radiation to a high degree. Residual radiation was parameterized with equations derived for SW radiation. Diurnal trends in radiation and other related meteorological parameters were evaluated.

For IR radiation, the Brunt Equation was found to adequately represent effective radiation without clouds. Attenuations (K-values) of 0.89, 0.64 and 0.51 were calculated for low, middle and high clouds, respectively. While the value for high clouds was high, the values for middle and low clouds were found to be similar to previous studies. A mean K-value of 0.80 for all cloud conditions was also determined and found to be within the same degree of accuracy as the individual K-values. In all cases, clouds were found to influence IR radiation better quadratically than linearly. The empirical equations used in this research were able to predict Wangara IR data to within 20-24%.

A modification of Beer's Law was derived to evaluate residual radiation under clear skies. An average turbidity coefficient of 0.16 was determined under the assumption that the surface albedo remained diurnally constant at 0.15. This value indicated a medium degree of turbidity as compared to values given by Flowers et al. (1969). Also,

similar to results by Robinson (1962), the optical air mass was found to cause an overestimation of the turbidity under low sun angles.

The cloud attenuation equation for SW radiation was found to represent the residual radiation adequately, although an analysis of attenuation coefficients, C-values, proved inconclusive. A C-value of 0.74 for low clouds at high solar angles was found to be in the range of previously published values; C-values at low solar angles and for middle and high clouds were unrealistically high.

Of considerable importance was the finding that cloud attenuation of residual radiation behaved nonlinearly. While solutions as high as the fourth order fit the data at noon, quadratic solutions fit well near sunset and sunrise. Overall, relative deviations during the day of the combined parameterization were approximately 20% at noon and just less than 30% for periods up to one hour before sunset or sunrise. Predictions within these one-hour periods, however, contained considerable error, partially due to the scatter and small magnitude of the measurements.

Diurnal trends in surface radiation and other meteorological parameters were established. The importance of the periods near sunset and sunrise was clearly evident since many important measurements changed sign or pattern at or near these time periods.

A comparison between surface radiation and the other three surface energy fluxes (sensible, latent and ground heat fluxes) was shown for a mean diurnal trend and under variations of clouds and wind speeds. A good correlation was observed between radiation and ground flux.

The Wangara data set offered an opportunity to use reliable, high resolution data to make, and verify, empirical predictions of the

surface radiation budget. Many relationships were established, but more studies with data of similar quality need to be completed before global parameterizations can be made with confidence.

REFERENCES

- Adem, J., 1967: On the relations between outgoing long-wave radiation, albedo and cloudiness. Mon. Wea. Rev., 95, 257-260.
- Bauer, K.G. and J.A. Dutton, 1962: Albedo variations measured from an airplane over several types of surface. J. Geophys. Res., 67, 2367-2376.
- Berlyand, T.G. (ed.), 1970: Teplovoi Balans. Lenengrad, Gidrometeorologicheskoe Press. (English transl.: Kathavate, 1975: Heat Balance, Washington D.C., Soil Conservation Service, 132 pp.)
- Brunt, D., 1932: Notes on radiation in the atmosphere. Quart. J. Roy. Met. Soc., 58, 389-420.
- _____, 1952: Physical and Dynamical Meteorology. Cambridge, Cambridge Univ. Press, 428 pp.
- Budyko, M.I., 1958: The Heat Balance of the Earth's Surface. Washington D.C., U.S. Weather Bureau, 599 pp. (Transl. from Russian.)
- Buettner, K.J.K. and C.D. Kern, 1965: The determination of infrared emissivities of terrestrial surfaces. J. Geophys. Res., 70, 1329-1337.
- Businger, J.A., J.C. Wyngaard, Y. Izumi and E.F. Bradley, 1971: Flux-profile relationships in the atmospheric surface layer. J. Atmos. Sci., 28, 181-189.
- Clark, R.H., 1970: Observational studies in the atmospheric boundary layer. Quart. J. Roy. Met. Soc., 96, 91-114.
- _____, A.J. Dyer, R.R. Brook, D.G. Reid and A.J. Troup, 1971: The Wangara Experiment: Boundary Layer Data. CSIRO Div. of Meteorol. Phys. Tech. Paper No. 19, 340 pp.
- _____, and G.D. Hess, 1973: On the appropriate scaling for velocity and temperature in the planetary boundary layer. J. Atmos. Sci., 30, 1346-1353.
- Deardorff, J.W., 1974: Three-dimensional numerical study of the height and mean structure of a heated planetary boundary layer. Boundary-Layer Meteorol., 7, 81-106.
- Dyer, A.J., B.B. Hicks and K.M. King, 1967: The fluxatron - a revised approach to the measurement of eddy fluxes in the lower atmosphere. J. Appl. Meteorol., 6, 408-413.
- Elliot, W.P., 1964: The height variation of vertical heat flux near the ground. Quart. J. Roy. Met. Soc., 90, 260-265.

- Estoque, M.A., 1963: A numerical model of the atmospheric boundary layer. J. Geophys. Res., 68, 1103-1113.
- Flowers, E.C., R.A. McCornick and K.R. Kurfis, 1969: Atmospheric turbidity over the United States, 1961-1966. J. Appl. Meteorol., 8, 955-962.
- Fritz, S., 1948: The albedo of the ground and atmosphere. Bull. Am. Meteorol. Soc., 29, 303-312.
- Fuchs, M. and C.B. Tanner, 1968: Surface temperature measurements of bare soils. J. Appl. Meteorol., 7, 303-305.
- Funk, J.P., 1959: Improved polythene-shielded net radiometer. J. Sci. Instrum., 36, 267-270.
- Geiger, R., 1959: The Climate Near the Ground. Cambridge, Harvard Press, 494 pp.
- Griggs, M.J., 1968: Emissivity of natural surfaces in the 8-14 micron spectral region. J. Geophys. Res., 73, 7546-7551.
- Halstead, M.H., R.L. Richman, W. Covoy and J.D. Merryman, 1957: A preliminary report on the design of a computer for micrometeorology. J. Meteorol., 14, 308-325.
- Haurwitz, B., 1948: Insolation in relation to cloud type. J. Meteorol., 5, 110-113.
- Hewson, E.W., 1943: The reflection, absorption and transmission of solar radiation by fog and cloud. Quart. J. Roy. Met. Soc., 69, 47-62.
- Houghton, H.G., 1954: On the annual heat balance of the northern hemisphere. J. Meteorol., 11, 1-9.
- _____, 1974: Physical Meteorology. Class notes, MIT, Cambridge, 350 pp.
- Hosler, C.R., 1961: Low-level inversion frequency in the contiguous United States. Mon. Wea. Rev., 89, 319-339.
- Kimball, H.H., 1919: Variations in the total and luminous solar radiation with geographical position in the United States. Mon. Wea. Rev., 47, 769-793.
- Kondratyev, K.Y., 1965: Actinometry. Washington D.C., National Aeronautics and Space Administration, 675 pp. (Transl. from Russian.)
- Kuhn, P.M. and V.E. Suomi, 1958: Airborne observations of albedo with a beam reflector. J. Meteorol., 15, 172-174.
- Kumar, A., 1978: A Simple Radiation Model for the Tar Sands Area. Edmonton, Syncrude Canada Ltd. Professional Paper 1978-3, 28 pp.

- Lettau, H.H. and B. Davidson, (eds.), 1957: Exploring the Atmosphere's First Mile. Vol. I and Vol. II. New York, Pergamon Press, 376 pp. and 578 pp.
- London, J. and T. Sasamori, 1971: Radiative energy budget of the atmosphere. In Man's Impact on Climate, Matthews, Kellogg and Robinson, (eds.), Cambridge, MIT Press, 141-155.
- Melgarejo, J.W. and J.W. Deardorff, 1974: Stability functions for the boundary-layer resistance laws based upon observed boundary-layer heights. J. Atmos. Sci., 31, 1324-1333.
- Obukhov, A.M., 1971: Turbulence in an atmosphere with a non-uniform temperature. Boundary-Layer Meteorol., 2, 7-29.
- Orlanski, I., B.B. Ross and L.J. Polinsky, 1974: Diurnal variation of the planetary boundary layer in a mesoscale model. J. Atmos. Sci., 31, 965-989.
- Panofski, H.A. and G.W. Brier, 1958: Some Applications of Statistics to Meteorology. University Park, Pennsylvania State University, 224 pp.
- Paulson, C.A., 1970: The mathematical representation of wind speed and temperature profiles in the unstable atmospheric surface layer. J. Appl. Meteorol., 9, 857-861.
- Philip, J.R., 1957: Evaporation, and moisture and heat fields in the soil. J. Meteorol., 14, 354-366.
- Pielke, R.A. and Y. Mahrer, 1975: Representation of the heated planetary boundary layer in mesoscale models with coarse vertical resolution. J. Atmos. Sci., 32, 2288-2308.
- Robinson, G.D., 1962: Absorption of solar radiation by atmospheric aerosol, as revealed by measurements at the ground. Archiv. Meteorol. Geophys. Bioklimatol. Ser. B, 12, 19-40.
- Rosenberg, N.J., 1974: Microclimate: The Biological Environment. New York, John Wiley and Sons, 315 pp.
- Sasamori, T. 1970: A numerical study of atmospheric and soil boundary layers. J. Atmos. Sci., 27, 1122-1137.
- Sellers, W.D., 1974: Physical Climatology. Chicago, The University of Chicago Press, 272 pp.
- Slade, D.H. (ed.), 1968: Meteorology and Atomic Energy, 1968. Washington D.C., Air Resources Lab., Department of Commerce, 445 pp.
- Swinbank, W.C. and A.J. Dyer, 1968: Micrometeorological Experiments 1962-1964. CSIRO Div. of Meteorol. Phys. Tech. Paper No. 17, 48 pp.

- Trewartha, G.T., 1968: An Introduction to Climate. New York, McGraw-Hill Inc., 408 pp.
- Turner, D.B., 1964: A diffusion model for an urban area. J. Appl. Meteorol.; 3, 83-91.
- Vonder Haar, T.H. and V.E. Suomi, 1969: Satellite observations of the earth's radiation budget. Science, 163, 667-669.
- _____ and _____, 1971: Measurements of the earth's radiation budget from satellites during a 5-year period. Part 1. Extended time and space means. J. Atmos. Sci., 28, 305-314.
- Wexler, H., 1934: Turbidities of American air masses and conclusions regarding the seasonal variation in atmospheric dust content. Mon. Wea. Rev., 62, 397-402.
- Yamada, T. and G. Mellor, 1975: A simulation of the Wangara atmospheric boundary layer data. J. Atmos. Sci., 32, 2309-2329.

APPENDIX

SENSIBLE HEAT FLUX CALCULATION

Methods for deriving sensible heat flux from near surface temperature and wind profiles have been developed by Businger et al. (1971) and Paulson (1970). These methods, which have their foundation in Monin-Obukhov Similarity theory, require horizontally uniform, flat terrain and assume fluxes to be constant with height in the lower boundary layer (lowest 50m). The procedure demonstrated in this section has been used by several researchers to simulate sensible heat flux for particular days of the Wangara Experiment (e.g.; Deardorff, 1974; Orlanski et al., 1974; Pielke and Mahrer, 1975 and Yamada and Mellor, 1975).

I. Equations

Sensible heat flux for positive values upwards can be written:

$$H_0 = -60\rho C_p u_* \theta_* (\text{ly min}^{-1}) \quad \text{A-1}$$

where air density $\rho = 1.3 \times 10^{-3} \text{ g cm}^{-3}$, specific heat of air at constant pressure $C_p = .24 \text{ cal g}^{-1} \text{ K}^{-1}$, u_* (cm/sec) is the friction velocity and θ_* (K) is a scaling temperature. (θ_* is negative, zero, and positive for unstable, neutral and stable lapse rates, respectively.)

Values of u_* and θ_* can be obtained from the integration of the nondimensional temperature, $\psi_h(z/L)$, and wind, $\phi_m(z/L)$, profiles where:

$$\psi_h(z/L) = \frac{kz}{\theta_*} \frac{\delta\theta}{\delta z} \quad \text{A-2}$$

and
$$\phi_m(z/L) = \frac{kz}{u_*} \frac{\delta u}{\delta z} \quad \text{A-3}$$

and k , the von Karman constant, is equal to 0.4.

Yamada and Mellor (1975) have adapted the solutions of the above integrations for the Wangara data as follows:

$$u_* = k U_m / [\ln(z_m/z_0) - \psi_m] \quad A-4$$

$$\text{and } \theta_* = 1.35 k (\theta_2 - \theta_1) / [\ln z_2/z_1 - \psi_h] \quad A-5$$

where it is suggested that $z_0 = 0.0012$ m (the roughness height). The subscript, m , reflects either an average height or a particular height where surface wind speed, U , is measured (0.5, 1, 2, 4, 8, 16 m). Values of θ_2 , θ_1 , z_2 , and z_1 are measured at the heights where the surface temperature gradient was obtained (2 and 1 m).

ψ_m and ψ_h are obtained for both stable ($\xi > 0$) and unstable ($\xi \leq 0$) flows from the integrals:

$$\psi_m = \int_0^{\xi_m} (1 - \phi_m) \xi^{-1} d\xi \quad A-6$$

$$\text{and } \psi_h = \int_{\xi_1}^{\xi_2} (1 - 1.35\phi_h) \xi^{-1} d\xi \quad A-7$$

where heights are the same as those used above and the variable ξ is defined as $\xi = z/L$. The Monin-Obukhov length, L , is expressed as:

$$L = \rho C_p \theta_0 u_*^3 / kg H_0 \quad A-8$$

where g is gravitational acceleration (9.8 m s^{-2}) and θ_0 is surface temperature calculated for the height, z_0 . The solutions to Eqs. A-6 and A-7 are:

$$\psi_m = \begin{cases} 2 \ln[(1+X)/2] + \ln[(1+X^2)/2] - 2 \tan^{-1}(X) + \pi/2 & \xi \leq 0 \\ -4.7 \xi_m & \xi > 0 \end{cases} \quad A-9$$

$$\psi_h = \begin{cases} 2 \ln[(1+Y_2)/(1+Y_1)] & \xi \leq 0 \\ -6.35 (\xi_2 - \xi_1) & \xi > 0 \end{cases} \quad A-10$$

Businger et al. (1971) found the values X and Y (1 or 2) to be:

$$X = (1-15\xi)^{\frac{1}{4}} \quad \text{A-11}$$

$$Y = (1-9\xi)^{\frac{1}{2}} \quad \text{A-12}$$

II. Procedure

All equations that are needed to calculate sensible heat flux for the Wangara data are now presented. Since the variable ξ must be initially estimated, the following procedure is given in three interative steps in order to obtain a better estimate of this value:

1. An initial estimate of L is made. It is assumed that the flow is stable at night, unstable during the day, and neutral near sunrise and sunset. Table A-1 exhibits the initial estimate for the Wangara data. These values were estimated with the aid of graphs found in Businger et al. (1971).

Table A-1. Initial Values of L (m).

Time (LST)	L
0100-0500, 2000-2400	3.
0600 & 1900	5.
0700 & 1800	999.
0800 & 1700	-999.
0900 & 1600	-5.
1000 - 1500	-1.

2. An average surface temperature gradient is obtained from the measured values between 1 and 2 m and 2 and 4 m.

3. The sign of L is changed if it does not conform to the stability of the flow. (L in negative for unstable temperature gradients.)

4. Equations A-9 and A-4 are evaluated for the wind speeds measured at heights of 0.5, 1, 2, and 4m.

5. An average value of u_x is determined from the four calculations.

6. Equations A-10 and A-5 are evaluated for the heights between 1 and 2 m. The temperature gradient determined in Step 2 is used for $\theta_2 - \theta_1$. A value of θ_x is obtained.

7. The sensible heat flux, H_0 , can now be calculated.

8. The Monin-Obukhov length is then redetermined (Eq. A-8).

9. Steps 4 through 7 are repeated two more times using this new value of L.

This procedure, for most cases studied, showed a convergence for L and H_0 after two or three calculations. Results for the sensible heat flux calculation are reasonable and are similar to previous calculations as discussed in Chapter 4.